Multichannel Group Sparsity Methods for Compressive Channel Estimation in Doubly Selective Multicarrier MIMO Systems

Daniel Eiwen[a], *Georg Tauböck*[b,c], *Franz Hlawatsch*[c], *and Hans Georg Feichtinger*[a]

[a]NuHAG, Faculty of Mathematics, University of Vienna, Austria ({daniel.eiwen,hans.feichtinger}@univie.ac.at)
[b]Acoustics Research Institute of the Austrian Academy of Sciences, Vienna, Austria (georg.tauboeck@oeaw.ac.at)
[c]Institute of Telecommunications, Vienna University of Technology, Austria (franz.hlawatsch@tuwien.ac.at)

arXiv:1407.3474v1 [cs.IT] 13 Jul 2014

Abstract

We consider compressive channel estimation within pulse-shaping multicarrier multiple-input multiple-output (MIMO) systems transmitting over doubly selective MIMO channels. This setup includes MIMO orthogonal frequency-division multiplexing (MIMO-OFDM) systems as a special case. We demonstrate that the individual component channels tend to exhibit an approximate *joint group sparsity* structure in the delay-Doppler domain. Motivated by this insight, we develop a compressive channel estimator that exploits the joint group sparsity structure for improved performance. The proposed channel estimator uses the methodology of multichannel group sparse compressed sensing (MGCS), which is derived by combining the existing methodologies of group sparse compressed sensing and multichannel compressed sensing. We derive an upper bound on the channel estimation error and analyze the estimator's computational complexity. The performance of the estimator is then further improved by replacing the Fourier basis used in the basic MGCS-based channel estimator by an alternative basis yielding enhanced joint group sparsity. We propose an iterative basis optimization algorithm that is able to utilize prior statistical information if available and amounts to a sequence of convex programming problems. Finally, simulations using a geometry-based channel simulator demonstrate the performance gains that can be achieved by leveraging the group sparsity, joint sparsity, and joint group sparsity of the component channels as well as the additional performance gains resulting from the use of the optimized basis.

Index Terms

Channel estimation, doubly selective channel, group basis pursuit denoising (G-BPDN), group-CoSaMP (G-CoSaMP), group orthogonal matching pursuit (G-OMP), group sparse compressed sensing, MIMO-OFDM, multicarrier modulation, multichannel compressed sensing, multiple-input multiple-output (MIMO) communications, orthogonal frequency-division multiplexing (OFDM), sparse reconstruction.

This work was supported by WWTF grant MA 07-004 (SPORTS) and by FWF grants S10602-N13 and S10603-N13 within the National Research Network SISE. This paper was presented in part at IEEE ICASSP 2010, Dallas, TX, Mar. 2010 and at IEEE SPAWC 2010, Marrakech, Morocco, June 2010.

Submitted to the IEEE Transactions on Information Theory, December 14, 2013.

I. Introduction

The growing demand for higher data rates in wireless communications has led to significant research on multiple-input multiple-output (MIMO) systems [1–3]. In this paper, we consider the estimation of doubly selective (doubly dispersive, doubly spread) MIMO channels based on the methodology of compressed sensing (CS) [4–7]. We focus on multicarrier (MC) MIMO systems, which include orthogonal frequency-division multiplexing (MIMO-OFDM) systems as a special case [8, 9]. MIMO-OFDM is a part of several important wireless standards like WLAN (IEEE 802.11n), fixed broadband wireless access (IEEE 802.16), and cellular communication systems (3GPP LTE, 4G) [10–13].

Coherent detection in MIMO wireless communication systems requires channel state information at the receiver. A common approach to obtaining channel state information is to embed pilot symbols into the transmit signal and to perform least-squares or minimum mean-square error channel estimation [14]; however, many more powerful channel estimation methods have been proposed (e.g., [15–22]). A challenging task is the design of the pilot symbols (values and patterns) [23–25].

Compressive channel estimation [26, 27] builds on the fact that doubly selective multipath channels tend to be dominated by a relatively small number of clusters of significant paths [28]. Compressive channel estimation uses CS techniques to exploit this inherent sparsity of the channel. The CS methodology enables the reconstruction of signals consisting of only few dominant components from far fewer measurements (samples) than is suggested by classical results [4–7]. However, available work on compressive channel estimation mostly focuses on single-input single-output (SISO) systems [26, 27, 29–31]. Previously proposed compressive channel estimation methods for MIMO systems [27, 32] exploit sparsity in the delay-Doppler-angle domain. By contrast, our approach to compressive channel estimation exploits the *joint* sparsity of the component channels in the delay-Doppler domain.

A major challenge in compressive channel estimation is posed by leakage effects, which are due to the finite bandwidth and blocklength of MC systems and strongly impair the effective delay-Doppler sparsity. In this paper, extending our previous work in [33] and [34], we make use of the recently introduced concept of *group sparsity* [35], which is closely related to *block sparsity* [36–38] and *model-based CS* [39], in order to exploit the delay-Doppler structure of leakage for improved channel estimation performance. Moreover, we show that, in typical scenarios, there is a strong similarity between the delay-Doppler sparsity patterns of the individual component channels of a MIMO system. We take advantage of this similarity by the use of *multichannel group sparse CS* (MGCS) methods, which combine the methodologies of *multichannel CS* (MCS) [40–44] and group sparse CS (GCS). We provide performance guarantees for the proposed MGCS-based channel estimators and

analyze their overall complexity.

Furthermore, to achieve a reduction of detrimental leakage effects, we propose to replace the discrete Fourier basis expansion used in conventional compressive channel estimation by a basis expansion that is optimum in the sense of maximizing the multichannel group sparsity underlying our MGCS channel estimator. The optimum basis is computed by an algorithm that extends our previous optimization procedures [26, 33, 34] to the case of multichannel group sparsity. The proposed basis optimization algorithm is able to take into account prior statistical information about the MIMO channel if available. We demonstrate experimentally that our MGCS-based channel estimators significantly outperform conventional compressive channel estimation for MIMO-OFDM systems, including the special case of SISO-OFDM systems, with large additional performance gains obtained from the use of the optimum basis.

The rest of this paper is organized as follows. The MC-MIMO system model is described in Section II. In Section III, we review GCS and MCS and combine them into the methodology of MGCS. In Section IV, the proposed MGCS channel estimator is presented and its performance and computational complexity are studied. In Section V, we analyze the multichannel group delay-Doppler sparsity of doubly selective MC-MIMO channels and investigate leakage effects. Section VI develops a basis expansion framework for enhancing multichannel group sparsity as well as an iterative algorithm for computing an optimized basis. Finally, in Section VII, we present experimental results that demonstrate the performance gains achieved by the proposed MGCS channel estimators and by the use of optimized basis expansions.

II. Multicarrier MIMO System Model

We consider a pulse-shaping MC-MIMO system for the sake of generality and because of its advantages over conventional cyclic-prefix (CP) MIMO-OFDM [45, 46]. However, CP MIMO-OFDM is included as a special case. The complex baseband is considered throughout.

A. Modulator, Channel, Demodulator

Let N_{T} and N_{R} denote the number of transmit and receive antennas, respectively. The modulator generates a discrete-time transmit signal vector $\mathbf{s}[n] \in \mathbb{C}^{N_{\mathrm{T}}}$ according to [45]

$$\mathbf{s}[n] \;=\; \sum_{l=0}^{L-1} \sum_{k=0}^{K-1} \mathbf{a}_{l,k}\, g_{l,k}[n]\,. \tag{1}$$

Here, L and K denote the number of transmitted MC-MIMO symbols and the number of subcarriers, respectively; $\mathbf{a}_{l,k} \triangleq \left(a_{l,k}^{(1)} \cdots a_{l,k}^{(N_{\mathrm{T}})}\right)^T \in \mathbb{C}^{N_{\mathrm{T}}}$ denotes the complex data symbol vectors; and $g_{l,k}[n] \triangleq g[n -$

$lN]\, e^{j2\pi \frac{k}{K}(n-lN)}$ is a time-frequency shift of a transmit pulse $g[n]$ ($N \geq K$ is the symbol duration). Subsequently, $\mathbf{s}[n]$ is converted into the continuous-time transmit signal vector

$$\mathbf{s}(t) \;=\; \sum_{n=-\infty}^{\infty} \mathbf{s}[n]\, f_1(t - nT_{\mathrm{s}})\,, \tag{2}$$

where $f_1(t)$ is the impulse response of an interpolation filter and T_{s} is the sampling period. Each transmit antenna $s \in \{1, \ldots, N_{\mathrm{T}}\}$ and receive antenna $r \in \{1, \ldots, N_{\mathrm{R}}\}$ are connected by a noisy, doubly selective channel with time-varying impulse response $h^{(r,s)}(t, \tau)$. The MIMO channel output can thus be written as [47, 48]

$$\mathbf{r}(t) \;=\; \int_{-\infty}^{\infty} \mathbf{H}(t, \tau)\, \mathbf{s}(t - \tau)\, d\tau \;+\; \mathbf{z}(t)\,, \tag{3}$$

where $\mathbf{H}(t, \tau)$ is the $N_{\mathrm{R}} \times N_{\mathrm{T}}$ matrix with entries $h^{(r,s)}(t, \tau)$ and $\mathbf{z}(t)$ is a noise vector. At the receiver, $\mathbf{r}(t)$ is converted to the discrete-time signal vector $\mathbf{r}[n] \in \mathbb{C}^{N_{\mathrm{R}}}$ according to

$$\mathbf{r}[n] \;=\; \int_{-\infty}^{\infty} \mathbf{r}(t)\, f_2(nT_{\mathrm{s}} - t)\, dt\,, \tag{4}$$

where $f_2(t)$ is the impulse response of an anti-aliasing filter. Subsequently, the demodulator computes

$$\mathbf{y}_{l,k} \;=\; \sum_{n=-\infty}^{\infty} \mathbf{r}[n]\, \gamma_{l,k}^{*}[n]\,, \qquad l \in \{0, \ldots, L-1\}\,,\; k \in \{0 \ldots, K-1\}\,, \tag{5}$$

where $\gamma_{l,k}[n] \triangleq \gamma[n - lN]\, e^{j2\pi \frac{k}{K}(n-lN)}$ is a time-frequency shift of a receive pulse $\gamma[n]$.

Combining equations (2)–(4), we obtain the following relation between the discrete-time vector signals $\mathbf{s}[n]$ and $\mathbf{r}[n]$:

$$\mathbf{r}[n] \;=\; \sum_{m=-\infty}^{\infty} \mathbf{H}[n, m]\, \mathbf{s}[n-m] \;+\; \mathbf{z}[n]\,, \tag{6}$$

where $\mathbf{H}[n, m] \triangleq \int_{-\infty}^{\infty} \int_{-\infty}^{\infty} \mathbf{H}(t + nT_{\mathrm{s}}, \tau)\, f_1(t - \tau + mT_{\mathrm{s}})\, f_2(-t)\, dt\, d\tau$ is a discrete-time time-varying impulse response matrix and $\mathbf{z}[n] \triangleq \int_{-\infty}^{\infty} \mathbf{z}(t) f_2(nT_{\mathrm{s}} - t)\, dt$ is discrete-time noise.

In the special case of a rectangular transmit pulse $g[n]$ and a rectangular receive pulse $\gamma[n]$ that are 1 on $\{0, \ldots, N-1\}$ and on $\{N-K, \ldots, N-1\}$, respectively and 0 otherwise, we obtain a conventional CP MIMO-OFDM system with CP length $N-K \geq 0$ [9, 13].

B. Equivalent Channel

It will be convenient to consider the equivalent MIMO channel that subsumes the MC modulator, interpolation filter, physical channel, anti-aliasing filter, and MC demodulator. Neglecting intersymbol and intercarrier

interference, which is justified if the channel dispersion is not too strong and if relevant system parameters are chosen appropriately [45, 46], equations (5), (6), and (1) yield

$$\mathbf{y}_{l,k} = \mathbf{H}_{l,k}\mathbf{a}_{l,k} + \mathbf{z}_{l,k}\,, \qquad l \in \{0,\ldots,L-1\}\,,\ k \in \{0,\ldots,K-1\}\,, \tag{7}$$

where the channel coefficient matrices $\mathbf{H}_{l,k} \in \mathbb{C}^{N_\mathrm{R}\times N_\mathrm{T}}$ are given by $\mathbf{H}_{l,k} \triangleq \sum_{n=-\infty}^{\infty}\sum_{m=-\infty}^{\infty}\mathbf{H}[n,m]\,g_{l,k}[n-m]\gamma_{l,k}^*[n]$; furthermore, $\mathbf{z}_{l,k} \triangleq \sum_{n=-\infty}^{\infty}\mathbf{z}[n]\gamma_{l,k}^*[n]$ [45].

Let $\gamma[n]$ be zero outside an interval $\{0,\ldots,L_\gamma\}$. To compute the $\mathbf{y}_{l,k}$ in (5), $\mathbf{r}[n]$ has to be known for $n \in \{0,\ldots,L_\mathrm{r}-1\}$, where $L_\mathrm{r} \triangleq (L-1)N + L_\gamma + 1$. For these n, (6) can be rewritten as

$$\mathbf{r}[n] \;=\; \sum_{m=-\infty}^{\infty}\sum_{i=0}^{L_\mathrm{r}-1}\mathbf{S}_h[m,i]\mathbf{s}[n-m]e^{j2\pi\frac{ni}{L_\mathrm{r}}} + \mathbf{z}[n]\,, \tag{8}$$

with the *discrete-delay-Doppler spreading function matrix* [47–49]

$$\mathbf{S}_h[m,i] \;\triangleq\; \frac{1}{L_\mathrm{r}}\sum_{n=0}^{L_\mathrm{r}-1}\mathbf{H}[n,m]e^{-j2\pi\frac{in}{L_\mathrm{r}}}\,, \qquad m,i \in \mathbb{Z}\,. \tag{9}$$

Let us assume that the channel is causal with maximum discrete delay at most $K-1$, i.e., $\mathbf{H}[n,m] = \mathbf{0}$ for $m \notin \{0,\ldots,K-1\}$. Then, using (5), (8), (1), and the approximation $L_\mathrm{r} \approx LN$ (which is exact for CP MIMO-OFDM), the channel coefficient matrices $\mathbf{H}_{l,k}$ can be expressed as

$$\mathbf{H}_{l,k} = \sum_{m=0}^{K-1}\sum_{i=-L/2}^{L/2-1}\mathbf{F}_{m,i}\,e^{-j2\pi(\frac{km}{K}-\frac{li}{L})}\,, \qquad l \in \{0,\ldots,L-1\}\,,\ k \in \{0,\ldots,K-1\}\,. \tag{10}$$

Here, L is assumed to be even for mathematical convenience and

$$\mathbf{F}_{m,i} \;\triangleq\; \sum_{q=0}^{N-1}\mathbf{S}_h[m,i+qL]\,A_{\gamma,g}^*\!\left(m,\frac{i+qL}{L_\mathrm{r}}\right), \tag{11}$$

where $A_{\gamma,g}(m,\xi) \triangleq \sum_{n=0}^{L_\gamma}\gamma[n]\,g^*[n-m]e^{-j2\pi\xi n}$ is the *cross-ambiguity function* of $\gamma[n]$ and $g[n]$ [50]. The matrices $\mathbf{F}_{m,i}$ provide a representation of the channel coefficient matrices $\mathbf{H}_{l,k}$ in terms of a discrete-delay variable m and a discrete-Doppler variable i.

III. Compressed Sensing of Jointly Group-Sparse Signals

In this section, we review some fundamentals of GCS [35–39] and MCS [40–44]. We then introduce the concept of *joint group sparsity* and a method for MGCS, which underlie the MIMO channel estimator presented in Section IV.

A. Group Sparse Compressed Sensing

The concepts of group sparsity and GCS extend the conventional concepts of sparsity and CS, respectively. We recall that a vector $\mathbf{x} \in \mathbb{C}^M$ is called (approximately) S-*sparse* if at most S of its entries are (approximately) nonzero. To define group sparsity, let $\mathcal{J} = \{\mathcal{I}_b\}_{b=1}^B$ be a partition of the index set $\{1, \ldots, M\}$ into "groups" $\mathcal{I}_b$, i.e., $\bigcup_{b=1}^B \mathcal{I}_b = \{1, \ldots, M\}$ and $\mathcal{I}_b \cap \mathcal{I}_{b'} = \emptyset$ for $b \neq b'$. For a vector $\mathbf{x} \in \mathbb{C}^M$, we define $\mathbf{x}[b] \in \mathbb{C}^{|\mathcal{I}_b|}$ to be the subvector of $\mathbf{x}$ comprising the entries $[\mathbf{x}]_j$ of $\mathbf{x}$ with $j \in \mathcal{I}_b$. Then $\mathbf{x}$ is called *group S-sparse with respect to $\mathcal{J}$* if at most S subvectors $\mathbf{x}[b]$ are not identically zero. The set of all such vectors $\mathbf{x}$ is denoted by $\Sigma_{S|\mathcal{J}}$. Note that an equivalent definition of group S-sparsity is that the vector $\big(\|\mathbf{x}[1]\|_2 \cdots \|\mathbf{x}[B]\|_2 \big)^T$ is S-sparse.

In a typical GCS scenario, we consider a linear model (or *measurement equation*)

$$\mathbf{y} = \mathbf{\Phi}\mathbf{x} + \mathbf{z}\,, \tag{12}$$

where $\mathbf{y} \in \mathbb{C}^Q$ is an observed vector of noisy measurements, $\mathbf{\Phi} \in \mathbb{C}^{Q \times M}$ is a known measurement matrix, $\mathbf{x} \in \mathbb{C}^M$ is an unknown vector that is known to be (approximately) group S-sparse with respect to a given partition $\mathcal{J}$, i.e., $\mathbf{x} \in \Sigma_{S|\mathcal{J}}$, and $\mathbf{z} \in \mathbb{C}^Q$ is an unknown noise vector. The indices b for which the $\mathbf{x}[b]$ are nonzero are unknown. Typically, the number of measurements is much smaller than the length of the vector, i.e., $Q \ll M$; thus, $\mathbf{\Phi}$ is a fat matrix. The goal is to reconstruct $\mathbf{x}$ from $\mathbf{y}$.

A trivial GCS reconstruction strategy is to use conventional CS techniques like basis pursuit denoising (BPDN) [51–53], orthogonal matching pursuit (OMP) [54–56], or compressive sampling matching pursuit (CoSaMP) [57], since a vector $\mathbf{x}$ that is group S-sparse with respect to some fixed partition $\mathcal{J}$ is also S'-sparse, where S' is the sum of the cardinalities of the S groups with largest cardinalities. However, this strategy does not leverage the group structure of $\mathbf{x}$. Therefore, some of the conventional CS recovery methods have been adapted to the group sparse case, as reviewed in what follows.

Let $\mathbf{x} \in \mathbb{C}^M$, not necessarily sparse or group sparse. We consider a partition $\mathcal{J} = \{\mathcal{I}_b\}_{b=1}^B$ of $\{1, \ldots, M\}$ and define an associated norm $\|\mathbf{x}\|_{2|\mathcal{J}} \triangleq \sum_{b=1}^B \|\mathbf{x}[b]\|_2$. The convex program

$$\min_{\mathbf{x}' \in \mathbb{C}^M} \|\mathbf{x}'\|_{2|\mathcal{J}} \qquad \text{subject to } \|\mathbf{\Phi}\mathbf{x}' - \mathbf{y}\|_2 \leq \epsilon \tag{13}$$

is called *group BPDN* (G-BPDN) [36, 37]. The accuracy of the solution of G-BPDN in approximating $\mathbf{x}$ can be estimated as follows. The measurement matrix $\mathbf{\Phi}$ is said to satisfy the *group restricted isometry property of order S with respect to $\mathcal{J}$* if there is a constant $\delta \in (0, 1)$ such that

$$(1-\delta)\|\tilde{\mathbf{x}}\|_2^2 \;\leq\; \|\mathbf{\Phi}\tilde{\mathbf{x}}\|_2^2 \;\leq\; (1+\delta)\|\tilde{\mathbf{x}}\|_2^2\,, \qquad \text{for all } \tilde{\mathbf{x}} \in \Sigma_{S|\mathcal{J}}\,. \tag{14}$$

The smallest such δ is denoted by $\delta_{S|\mathcal{J}}$ and is called the *group restricted isometry constant of order S with respect to $\mathcal{J}$* (abbreviated as G-RIC) [36]. Let $\hat{\mathbf{x}}$ denote the solution of (13), and let $\mathbf{x}^{S|\mathcal{J}}$ denote the best group S-sparse approximation of $\mathbf{x}$ with respect to $\mathcal{J}$, i.e., the $\mathbf{x}' \in \Sigma_{S|\mathcal{J}}$ minimizing $\|\mathbf{x}'-\mathbf{x}\|_{2|\mathcal{J}}$. As shown in [36], if $\mathbf{y}$ satisfies $\|\mathbf{\Phi x}-\mathbf{y}\|_2 = \|\mathbf{z}\|_2 \leq \epsilon$ and $\mathbf{\Phi}$ satisfies the group restricted isometry property of order $2S$ with G-RIC $\delta_{2S|\mathcal{J}} \leq \sqrt{2}-1$, then[1]

$$\|\hat{\mathbf{x}}-\mathbf{x}\|_2 \;\leq\; \frac{c_0}{\sqrt{S}}\,\|\mathbf{x}-\mathbf{x}^{S|\mathcal{J}}\|_{2|\mathcal{J}} + c_1\epsilon\,, \tag{15}$$

where $c_0 = \frac{2\,(1-\delta_{2S|\mathcal{J}})}{1-(1+\sqrt{2})\,\delta_{2S|\mathcal{J}}}$ and $c_1 = \frac{4\sqrt{1+\delta_{2S|\mathcal{J}}}}{1-(1+\sqrt{2})\,\delta_{2S|\mathcal{J}}}$. This result bounds the reconstruction error $\|\hat{\mathbf{x}}-\mathbf{x}\|_2$ in terms of $\|\mathbf{x}-\mathbf{x}^{S|\mathcal{J}}\|_{2|\mathcal{J}}$, which characterizes the deviation of $\mathbf{x}$ from being group S-sparse with respect to $\mathcal{J}$, and in terms of ϵ.

An alternative GCS reconstruction technique is *group OMP* (G-OMP; usually called block OMP) [38, 58, 59]. This is a greedy algorithm that iteratively identifies the support of the unknown vector. In each iteration, the current support estimate is extended by an entire group of $\mathcal{J}$ (whereas in conventional OMP, only a single index is added). Although G-OMP often outperforms G-BPDN in practice, performance guarantees are only available for exactly group sparse vectors.

To bridge this gap, we will specialize the model-based CoSaMP algorithm [39] to the group sparse setting. The resulting GCS algorithm, which we abbreviate as G-CoSaMP, is a greedy algorithm that differs from the classical CoSaMP algorithm in that, in each iteration, the support estimate is adapted in terms of entire groups of $\mathcal{J}$ instead of single indices. Specializing results from [39], the performance of G-CoSaMP can be characterized as follows. Consider a partition $\mathcal{J}$ with groups of equal size. If $\mathbf{y}$ satisfies $\|\mathbf{\Phi x}-\mathbf{y}\|_2 \leq \epsilon$ and $\mathbf{\Phi}$ satisfies the group restricted isometry property of order $4S$ with respect to $\mathcal{J}$ with G-RIC $\delta_{4S|\mathcal{J}} \leq 0.1$, the result $\hat{\mathbf{x}}$ of G-CoSaMP after n iteration steps satisfies[2]

$$\|\hat{\mathbf{x}}-\mathbf{x}\|_2 \;\leq\; \frac{1}{2^n}\,\|\mathbf{x}\|_2 + 20\left(1+\frac{1}{\sqrt{S}}\right)\|\mathbf{x}-\mathbf{x}^{S|\mathcal{J}}\|_{2|\mathcal{J}} + 20\epsilon\,. \tag{16}$$

We recall that a matrix $\mathbf{\Phi}$ satisfies the conventional restricted isometry property of order S' with restricted isometry constant (RIC) $\delta_{S'}$ if the double inequality in (14) is satisfied for every S'-sparse vector $\tilde{\mathbf{x}}$ [52, 60, 61]

[1] We note that this result was formulated in [36] for the special case of block sparsity; however, it extends to the general group sparse setting in a straightforward way.

[2] Here, we have used the inequality $\|\mathbf{x}\|_2 \leq \|\mathbf{x}\|_{2|\mathcal{J}}$, which can be shown as follows:

$$\|\mathbf{x}\|_2 \;=\; \sqrt{\sum_{b=1}^{B}\sum_{j\in\mathcal{I}_b}\left|[\mathbf{x}]_j\right|^2} \;\leq\; \sum_{b=1}^{B}\sqrt{\sum_{j\in\mathcal{I}_b}\left|[\mathbf{x}]_j\right|^2} \;=\; \sum_{b=1}^{B}\|\mathbf{x}[b]\|_2 \;=\; \|\mathbf{x}\|_{2|\mathcal{J}}\,.$$

(and $\delta_{S'}$ is the smallest δ in (14)). Since, as observed earlier, a vector that is group S-sparse with respect to some fixed partition $\mathcal{J}$ is also S'-sparse, where S' is the sum of the cardinalities of the S groups with largest cardinalities, the G-RIC of $\mathbf{\Phi}$ satisfies $\delta_{S|\mathcal{J}} \leq \delta_{S'}$. The following result has been shown in [62], cf. also [6, 63, 64]. Let $\mathbf{\Phi}$ be a $Q \times M$ matrix that is constructed by choosing uniformly at random Q rows from a unitary $M \times M$ matrix $\mathbf{U}$ and properly scaling the resulting matrix. Then for any prescribed $\gamma \in (0,1)$ and $\eta \in (0,1)$, $\mathbf{\Phi}$ will, with probability at least $1-\eta$, satisfy the restricted isometry property of order S' with RIC $\delta_{S'} < \gamma$ if

$$Q \geq C \, \frac{\mu_{\mathbf{U}}^2 S' \max\{\log^3(S') \log(M), \log(1/\eta)\}}{\gamma^2}, \tag{17}$$

where C is a constant and $\mu_{\mathbf{U}} \triangleq \sqrt{M} \max_{i,j} |[\mathbf{U}]_{i,j}|$. Clearly, if $\delta_{S'} < \gamma$, also $\delta_{S|\mathcal{J}} < \gamma$. Unfortunately, there are so far no results that improve on the above result by exploiting the available group structure.

B. Multichannel Compressed Sensing

Let $\Theta \triangleq \{\theta_1, \theta_2, \ldots, \theta_{|\Theta|}\}$ be a finite index set. A collection of vectors $\mathbf{x}^{(\theta)} \in \mathbb{C}^M$, $\theta \in \Theta$ is called *jointly S-sparse* if the $\mathbf{x}^{(\theta)}$ share a common S-sparse support, i.e., $\big|\bigcup_{\theta \in \Theta} \operatorname{supp}(\mathbf{x}^{(\theta)})\big| \leq S$ with $\operatorname{supp}(\mathbf{x}^{(\theta)}) \triangleq \big\{j \in \{1, \ldots, M\} \,\big|\, [\mathbf{x}^{(\theta)}]_j \neq 0\big\}$. We consider the *simultaneous sparse reconstruction problem*, where the unknown, (approximately) jointly S-sparse vectors $\mathbf{x}^{(\theta)} \in \mathbb{C}^M$, $\theta \in \Theta$ are to be reconstructed simultaneously from measurements vectors $\mathbf{y}^{(\theta)} \in \mathbb{C}^Q$ given by

$$\mathbf{y}^{(\theta)} = \mathbf{\Phi}^{(\theta)} \mathbf{x}^{(\theta)} + \mathbf{z}^{(\theta)}, \quad \theta \in \Theta. \tag{18}$$

Here, the $\mathbf{\Phi}^{(\theta)} \in \mathbb{C}^{Q \times M}$ are known measurement matrices and the $\mathbf{z}^{(\theta)} \in \mathbb{C}^Q$ are unknown noise vectors. The supports $\operatorname{supp}(\mathbf{x}^{(\theta)})$ are unknown, and typically $Q \ll M$. Thus, the $\mathbf{\Phi}^{(\theta)}$ are fat matrices. Note that the conventional sparse reconstruction problem is reobtained for $|\Theta| = 1$.

Because each vector $\mathbf{x}^{(\theta)}$ is itself (approximately) S-sparse, any conventional CS method, such as BPDN, OMP, or CoSaMP, can be used to reconstruct each vector individually. However, this trivial MCS approach does not profit from the common structure of the vectors. Therefore, some CS methods have been adapted to the case of jointly sparse vectors. For example, *distributed compressed sensing — simultaneous OMP* (DCS-SOMP) [44] produces very good results in practice, and for *CoSOMP* [65], performance guarantees are available. For the special case where all measurement matrices coincide, i.e., $\mathbf{\Phi}^{(\theta)} = \mathbf{\Phi}$ for all $\theta \in \Theta$, *multichannel BPDN* (M-BPDN) [40, 42, 66] and *simultaneous OMP* (SOMP) [41, 43] are probably the most popular MCS methods.

C. Multichannel Group Sparse Compressed Sensing

We now combine the notions of group sparsity and joint sparsity. We call a collection of vectors $\mathbf{x}^{(\theta)} \in \mathbb{C}^M$, $\theta \in \Theta$ *jointly group S-sparse with respect to the partition* $\mathcal{J} = \{\mathcal{I}_b\}_{b=1}^B$ if the vectors $\left(\left\|\mathbf{x}^{(\theta)}[1]\right\|_2 \cdots \left\|\mathbf{x}^{(\theta)}[B]\right\|_2 \right)^T$, $\theta \in \Theta$ are jointly S-sparse. Furthermore, we consider the *simultaneous group sparse reconstruction problem*, i.e., the problem of reconstructing vectors $\mathbf{x}^{(\theta)}$, $\theta \in \Theta$ that are (approximately) jointly group S-sparse with respect to a given partition $\mathcal{J}$ from the observations $\mathbf{y}^{(\theta)}$, $\theta \in \Theta$ given by (18). Once again, we could use a conventional CS technique for each vector $\mathbf{x}^{(\theta)}$ individually, since each $\mathbf{x}^{(\theta)}$ is (approximately) S'-sparse, where S' is the sum of the cardinalities of the S groups with largest cardinalities (cf. Section III-A). Alternatively, we could use a GCS technique for each $\mathbf{x}^{(\theta)}$, since each $\mathbf{x}^{(\theta)}$ is itself (approximately) group S-sparse with respect to $\mathcal{J}$. Finally, we could use an MCS technique since the $\mathbf{x}^{(\theta)}$ are (approximately) jointly S'-sparse. However, none of these trivial MGCS approaches fully leverages the combined group sparsity and joint sparsity.

Therefore, we next propose a method for simultaneous group sparse reconstruction that overcomes these limitations. Our approach is based on the well-known fact that, using a stacking as explained later, the simultaneous sparse reconstruction problem can be recast as a group sparse reconstruction problem [36, 65]. We will extend this principle to the simultaneous *group* sparse reconstruction problem. Let the vectors $\mathbf{x}^{(\theta)} \in \mathbb{C}^M$, $\theta \in \Theta$ be jointly group S-sparse with respect to the partition $\mathcal{J} = \{\mathcal{I}_b\}_{b=1}^B$ of $\{1, \ldots, M\}$. Then, we consider the associated index set $\{1, \ldots, M|\Theta|\}$, and we define an associated partition $\tilde{\mathcal{J}} \triangleq \{\tilde{\mathcal{I}}_b\}_{b=1}^B$ of $\{1, \ldots, M|\Theta|\}$ with groups $\tilde{\mathcal{I}}_b$ of size $|\tilde{\mathcal{I}}_b| = |\mathcal{I}_b||\Theta|$ given by

$$\tilde{\mathcal{I}}_b \triangleq \left\{ j + (\xi - 1)M \,\middle|\, j \in \mathcal{I}_b, \xi \in \{1, \ldots, |\Theta|\} \right\}. \tag{19}$$

Furthermore, we stack the $\mathbf{x}^{(\theta)}$ into the vector $\mathbf{x} \triangleq \left(\mathbf{x}^{(\theta_1)T} \cdots \mathbf{x}^{(\theta_{|\Theta|})T}\right)^T$ of length $M|\Theta|$ and the $\mathbf{y}^{(\theta)}$ into the vector $\mathbf{y} \triangleq \left(\mathbf{y}^{(\theta_1)T} \cdots \mathbf{y}^{(\theta_{|\Theta|})T}\right)^T$ of length $Q|\Theta|$, and we define the following block-diagonal matrix of size $Q|\Theta| \times M|\Theta|$:

$$\mathbf{\Phi} \triangleq \begin{pmatrix} \mathbf{\Phi}^{(\theta_1)} & & \mathbf{0} \\ & \ddots & \\ \mathbf{0} & & \mathbf{\Phi}^{(\theta_{|\Theta|})} \end{pmatrix}. \tag{20}$$

Then, the equations (18) can be written in the form of (12), i.e.,

$$\mathbf{y} = \mathbf{\Phi}\mathbf{x} + \mathbf{z}, \tag{21}$$

with $\mathbf{z} \triangleq \left(\mathbf{z}^{(\theta_1)T} \cdots \mathbf{z}^{(\theta_{|\Theta|})T}\right)^T$. It is now easily verified that

$$\mathbf{x}[b] = \left(\left(\mathbf{x}^{(\theta_1)}[b]\right)^T \cdots \left(\mathbf{x}^{(\theta_{|\Theta|})}[b]\right)^T\right)^T, \qquad b \in \{1, \ldots, B\}. \tag{22}$$

(Note that the b on the left-hand side refers to the partition $\tilde{\mathcal{J}}$ whereas the b on the right-hand side refers to the partition $\mathcal{J}$.) Therefore, if the vectors $\mathbf{x}^{(\theta)}$ are jointly group S-sparse with respect to $\mathcal{J}$, the stacked vector $\mathbf{x}$ is group S-sparse with respect to $\tilde{\mathcal{J}}$. Therefore, by applying a reconstruction method for GCS—such as G-BPDN, G-OMP, or G-CoSaMP—to (21), we can fully exploit the structure given by the simultaneous group sparsity and joint sparsity of the $\mathbf{x}^{(\theta)}$. (We will say that the respective GCS reconstruction method "operates in MGCS mode.") It is furthermore easy to show that the G-RIC of $\mathbf{\Phi}$ with respect to $\tilde{\mathcal{J}}$, denoted $\delta_{S|\tilde{\mathcal{J}}}$, satisfies

$$\delta_{S|\tilde{\mathcal{J}}} \;=\; \max_{\theta\in\Theta} \delta^{(\theta)}_{S|\mathcal{J}}\,, \tag{23}$$

where $\delta^{(\theta)}_{S|\mathcal{J}}$ is the G-RIC of $\mathbf{\Phi}^{(\theta)}$ with respect to $\mathcal{J}$.

Finally, an alternative approach to solving the simultaneous group sparse reconstruction problem is to modify existing reconstruction methods for MCS to additionally incorporate group sparsity. For DCS-SOMP (see Section III-B) this can be done easily. The resulting G-DCS-SOMP algorithm simply adds entire groups to the joint support in each iteration, rather than adding only single indices.

IV. Compressive MIMO Channel Estimation Exploiting Joint Group Sparsity

In this section, we propose an MGCS-based MC-MIMO channel estimator that exploits joint group sparsity. This estimator generalizes the estimators previously presented in [26, 33, 34]. The joint group sparsity structure of doubly selective MC-MIMO channels will be motivated and studied in Section V.

A. Subsampled Time-Frequency Grid and Pilot Arrangement

Let $\theta \triangleq (r,s)$ index the channel between transmit antenna s and receive antenna r, and let $\Theta \triangleq \big\{\theta = (r,s)\,|\,r\in\{1,\dots,N_{\mathrm{R}}\},\, s\in\{1,\dots,N_{\mathrm{T}}\}\big\}$ be the set of all channel indices. For real-world (underspread [47, 48]) wireless channels and practical transmit and receive pulses, the entries $F^{(\theta)}_{m,i} \triangleq [\mathbf{F}_{m,i}]_{r,s}$ of the matrices $\mathbf{F}_{m,i}$ in (11) are effectively supported in some small rectangular region about the origin of the discrete delay-Doppler ((m,i)) plane. Thus, in what follows, we assume that the support of $\mathbf{F}_{m,i}$ is contained in $\{0,\dots,D-1\}\times\{-J/2,\dots,J/2-1\}$ (within the fundamental i-period), where D and J are chosen such that D divides K and J divides L, i.e., $\Delta K \triangleq K/D$ and $\Delta L \triangleq L/J$ are integers, and J (and therefore also L) is assumed even for mathematical convenience. Because of the two-dimensional (2D) discrete Fourier transform (DFT) relation—strictly speaking, DFT/inverse DFT relation—in (10), the channel coefficient matrices $\mathbf{H}_{l,k}$ are then uniquely determined by their values on the *subsampled time-frequency grid*

$$\mathcal{G} \triangleq \big\{(l,k) = (\lambda\,\Delta L, \kappa\,\Delta K)\,\big|\,\lambda\in\{0,\dots,J-1\},\ \kappa\in\{0,\dots,D-1\}\big\}\,.$$

Due to (10), these subsampled values are given by

$$\mathbf{H}_{\lambda\,\Delta L,\kappa\,\Delta K} \;=\; \sum_{m=0}^{D-1}\sum_{i=-J/2}^{J/2-1} \mathbf{F}_{m,i}\, e^{-j2\pi(\frac{\kappa m}{D}-\frac{\lambda i}{J})}. \tag{24}$$

We will show in Section V that the $F_{m,i}^{(\theta)}$ for all $\theta\in\Theta$, considered as functions of m and i, can be assumed jointly group sparse. More precisely, we will show that the vectors $\mathrm{rvec}_{m,i}\{F_{m,i}^{(\theta)}\} \triangleq \big(F_{0,-J/2}^{(\theta)}\;F_{0,-J/2+1}^{(\theta)}\cdots F_{1,-J/2}^{(\theta)} \cdots F_{D-1,J/2-1}^{(\theta)}\big)^T$, $\theta\in\Theta$ that are obtained by a rowwise stacking with respect to m,i of the $D\times J$ "matrices" $F_{m,i}^{(\theta)}$ into JD-dimensional vectors, are approximately jointly group sparse with respect to some partition $\mathcal{J}$; however, the sparsity level is strongly affected by leakage effects. In order to reduce the leakage effects inherent to the 2D DFT expansion (24) and, thereby, improve the joint group sparsity of the $F_{m,i}^{(\theta)}$, we generalize (24) to an orthonormal 2D basis expansion

$$\mathbf{H}_{\lambda\,\Delta L,\kappa\,\Delta K} \;=\; \sum_{m=0}^{D-1}\sum_{i=-J/2}^{J/2-1} \mathbf{G}_{m,i}\, u_{m,i}[\lambda,\kappa]\,, \tag{25}$$

with a suitably chosen orthonormal 2D basis $\{u_{m,i}[\lambda,\kappa]\}$. The construction of a basis yielding an improved joint group sparsity of the entries $G_{m,i}^{(\theta)} \triangleq [\mathbf{G}_{m,i}]_{r,s}$ will be explained in Section VI. Clearly, the 2D DFT (24) is a special case of (25) with $\mathbf{G}_{m,i} = \sqrt{JD}\,\mathbf{F}_{m,i}$ and $u_{m,i}[\lambda,\kappa] = \frac{1}{\sqrt{JD}}\, e^{-j2\pi(\frac{\kappa m}{D}-\frac{\lambda i}{J})}$.

Let $\mu \triangleq (l,k)$ index the (nonsubsampled) time-frequency positions. For pilot-aided channel estimation, we choose N_{T} linearly independent pilot vectors $\mathbf{p}^{(s)} \triangleq \big(p_1^{(s)}\cdots p_{N_{\mathrm{T}}}^{(s)}\big)^T$, $s\in\{1,\ldots,N_{\mathrm{T}}\}$ as well as N_{T} pairwise disjoint sets of pilot time-frequency positions $\mathcal{P}^{(s)}$, $s\in\{1,\ldots,N_{\mathrm{T}}\}$. The pilot position sets $\mathcal{P}^{(s)}$ are subsets of the subsampled time-frequency grid $\mathcal{G}$, i.e., $\mathcal{P}^{(s)}\subseteq\mathcal{G}$, and they have equal size $Q \triangleq |\mathcal{P}^{(s)}|$. Let $\mu_q^{(s)}$, $q\in\{1,\ldots,Q\}$ denote the pilot time-frequency positions in $\mathcal{P}^{(s)}$. For each $s\in\{1,\ldots,N_{\mathrm{T}}\}$, the pilot vector $\mathbf{p}^{(s)}$ is transmitted at all Q time-frequency positions $\mu_q^{(s)}\in\mathcal{P}^{(s)}$, i.e., we have $\mathbf{a}_{\mu_q^{(s)}}=\mathbf{p}^{(s)}$ for all $q\in\{1,\ldots,Q\}$ in (1). Thus, $N_{\mathrm{T}}Q$ pilot vectors, or N_{T}^2Q pilots symbols, are transmitted in total. An example of such a pilot arrangement is shown in Figure 1. Note that the individual entries of the vector $\mathbf{a}_{\mu_q^{(s)}} = \mathbf{p}^{(s)}$ correspond to pilots at the same time-frequency position, but transmitted from different antennas.

B. The Estimator

Let $y_\mu^{(r)} \triangleq [\mathbf{y}_\mu]_r$ (cf. (5)) denote the demodulated symbol at receive antenna r and time-frequency position μ, with $z_\mu^{(r)} \triangleq [\mathbf{z}_\mu]_r$ (cf. (7)) the associated noise component. Furthermore let

$$\tilde{G}_{m,i}^{(\theta)} \;\triangleq\; \mathbf{g}_{m,i}^{(r)T}\,\mathbf{p}^{(s)}, \tag{26}$$

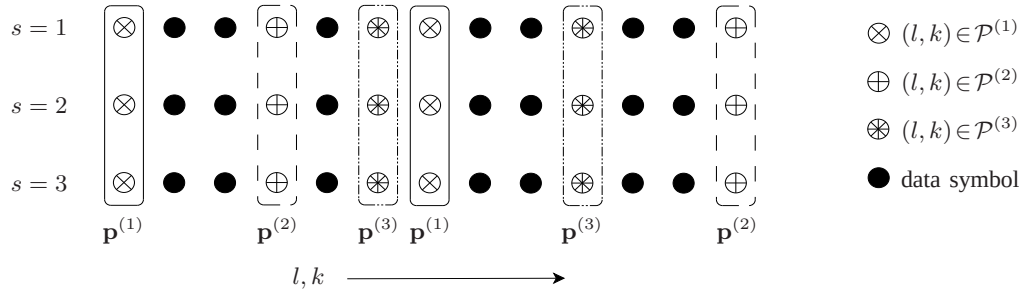

Fig. 1. Example of a pilot setup for an MC-MIMO system with $N_{\mathrm{T}}=3$ transmit antennas. For each $s\in\{1,2,3\}$, the same length-3 pilot vector $\mathbf{p}^{(s)}$ is transmitted at all time-frequency positions $(l,k)\in\mathcal{P}^{(s)}$. Note that $Q=|\mathcal{P}^{(s)}|=2$.

where $\mathbf{g}_{m,i}^{(r)T}$ denotes the rth row of $\mathbf{G}_{m,i}$ and, as before, $\theta=(r,s)$. Then, writing $\mu_q^{(s)}\triangleq(\lambda_q^{(s)}\Delta L,\kappa_q^{(s)}\Delta K)$ for the pilot time-frequency positions, we obtain

$$\begin{aligned}
y_{\mu_q^{(s)}}^{(r)} &= \big[\mathbf{y}_{\mu_q^{(s)}}\big]_r \\
&\overset{(7)}{=} \big[\mathbf{H}_{\mu_q^{(s)}}\mathbf{p}^{(s)}+\mathbf{z}_{\mu_q^{(s)}}\big]_r \\
&\overset{(25)}{=} \left[\left(\sum_{m=0}^{D-1}\sum_{i=-J/2}^{J/2-1}\mathbf{G}_{m,i}\,u_{m,i}\big[\lambda_q^{(s)},\kappa_q^{(s)}\big]\right)\mathbf{p}^{(s)}+\mathbf{z}_{\mu_q^{(s)}}\right]_r \\
&= \sum_{m=0}^{D-1}\sum_{i=-J/2}^{J/2-1}\mathbf{g}_{m,i}^{(r)T}\,\mathbf{p}^{(s)}\,u_{m,i}\big[\lambda_q^{(s)},\kappa_q^{(s)}\big]+z_{\mu_q^{(s)}}^{(r)} \\
&\overset{(26)}{=} \sum_{m=0}^{D-1}\sum_{i=-J/2}^{J/2-1}\tilde{G}_{m,i}^{(\theta)}\,u_{m,i}\big[\lambda_q^{(s)},\kappa_q^{(s)}\big]+z_{\mu_q^{(s)}}^{(r)},
\end{aligned}\tag{27}$$

for all $q\in\{1,\ldots,Q\}$, $s\in\{1,\ldots,N_{\mathrm{T}}\}$, and $r\in\{1,\ldots,N_{\mathrm{R}}\}$. To rewrite this relation in vector-matrix notation, we define $\mathbf{U}$ to be the unitary $JD\times JD$ matrix whose $(mJ+i+J/2+1)$th column is given by $\mathrm{rvec}_{\lambda,\kappa}\big\{u_{m,i}[\lambda,\kappa]\big\}=\big(u_{m,i}[0,0]\;\;u_{m,i}[0,1]\cdots u_{m,i}[1,0]\cdots u_{m,i}[J-1,D-1]\big)^T$ (this denotes the rowwise stacking with respect to λ,κ of the $J\times D$ "matrix" $u_{m,i}[\lambda,\kappa]$ into a JD-dimensional vector). Furthermore, we set

$$\mathbf{\Phi}^{(s)}\triangleq\sqrt{\frac{JD}{Q}}\,\mathbf{U}^{(s)}\in\mathbb{C}^{Q\times JD},\tag{28}$$

where $\mathbf{U}^{(s)}$ denotes the $Q\times JD$ submatrix of $\mathbf{U}$ constituted by the Q rows corresponding to the pilot positions $\mu_q^{(s)}\in\mathcal{P}^{(s)}$, $q\in\{1,\ldots,Q\}$. We also define the vectors

$$\mathbf{x}^{(\theta)}\triangleq\sqrt{\frac{Q}{JD}}\,\mathrm{rvec}_{m,i}\big\{\tilde{G}_{m,i}^{(\theta)}\big\}\in\mathbb{C}^{JD},\tag{29}$$

as well as the vectors $\mathbf{y}^{(\theta)}\triangleq\big(y_1^{(\theta)}\cdots y_Q^{(\theta)}\big)^T\in\mathbb{C}^Q$ with $y_q^{(\theta)}\triangleq y_{\mu_q^{(s)}}^{(r)}$ and $\mathbf{z}^{(\theta)}\triangleq\big(z_1^{(\theta)}\cdots z_Q^{(\theta)}\big)^T\in\mathbb{C}^Q$ with $z_q^{(\theta)}\triangleq z_{\mu_q^{(s)}}^{(r)}$. We can then rewrite (27) as

$$\mathbf{y}^{(\theta)} = \mathbf{\Phi}^{(s)}\mathbf{x}^{(\theta)} + \mathbf{z}^{(\theta)}, \qquad \theta = (r,s) \in \Theta\,. \tag{30}$$

Thus, we have obtained measurement equations of the form (18), of dimension $Q \times JD$. In practice, $Q \ll JD$. Since we assumed the coefficients $G_{m,i}^{(\theta)}$ to be (approximately) jointly group sparse, the functions $\tilde{G}_{m,i}^{(\theta)} = \mathbf{g}_{m,i}^{(r)T}\mathbf{p}^{(s)}$, and consequently the vectors $\mathbf{x}^{(\theta)}$, are (approximately) jointly group sparse. Therefore, (30) is recognized as an instance of the MGCS problem introduced in Section III-C, and thus any MGCS reconstruction algorithm can be used to reconstruct the $\mathbf{x}^{(\theta)}$.

We can now state the overall channel estimation algorithm as follows:

1) Stack the demodulated symbols at the pilot positions, $y_{\mu_q^{(s)}}^{(r)}$, into the vectors $\mathbf{y}^{(\theta)}$ as described above, and use an MGCS reconstruction algorithm (based on the measurement matrices $\mathbf{\Phi}^{(s)}$) to obtain estimates $\hat{\mathbf{x}}^{(\theta)}$ of the vectors $\mathbf{x}^{(\theta)}$.
2) Rescale these estimates $\hat{\mathbf{x}}^{(\theta)}$ with $\sqrt{\frac{JD}{Q}}$ to obtain estimates $\hat{\tilde{G}}_{m,i}^{(\theta)}$ of $\tilde{G}_{m,i}^{(\theta)}$, i.e., calculate $\mathrm{rvec}_{m,i}\{\hat{\tilde{G}}_{m,i}^{(\theta)}\} = \sqrt{\frac{JD}{Q}}\hat{\mathbf{x}}^{(\theta)}$ (cf. (29)).
3) Calculate (cf. (26))

$$\hat{\mathbf{g}}_{m,i}^{(r)} = \mathbf{P}^{-T}\big(\hat{\tilde{G}}_{m,i}^{(r,1)} \cdots \hat{\tilde{G}}_{m,i}^{(r,N_\mathrm{T})}\big)^T, \qquad \text{with } \mathbf{P} \triangleq \big(\mathbf{p}^{(1)} \cdots \mathbf{p}^{(N_\mathrm{T})}\big)\,.$$

   Note that the matrix $\mathbf{P}$ is nonsingular since the pilot vectors $\mathbf{p}^{(s)}$ were chosen linearly independent.
4) From $\hat{\mathbf{g}}_{m,i}^{(r)}$, calculate estimates $\hat{\mathbf{H}}_{\lambda\,\Delta L,\kappa\,\Delta K}$ of the subsampled channel coefficient matrices $\mathbf{H}_{\lambda\,\Delta L,\kappa\,\Delta K}$ according to (25) with $\mathbf{G}_{m,i}$ replaced by $\hat{\mathbf{G}}_{m,i}$.
5) Calculate estimates of the 2D DFT coefficients $\mathbf{F}_{m,i}$ according to the inversion of (24), i.e.,

$$\hat{\mathbf{F}}_{m,i} = \begin{cases} \dfrac{1}{JD}\displaystyle\sum_{\lambda=0}^{J-1}\sum_{\kappa=0}^{D-1} \hat{\mathbf{H}}_{\lambda\,\Delta L,\kappa\,\Delta K}\, e^{-j2\pi(\frac{i\lambda}{J}-\frac{m\kappa}{D})}, & m \in \{0,\dots,D-1\},\ i \in \{-J/2,\dots,J/2-1\} \\ \mathbf{0}\,, & \text{otherwise.} \end{cases} \tag{31}$$

6) Calculate estimates $\hat{\mathbf{H}}_{l,k}$ of all channel coefficient matrices $\mathbf{H}_{l,k}$ by using the 2D DFT expansion (10) with $\mathbf{F}_{m,i}$ replaced by $\hat{\mathbf{F}}_{m,i}$.

In the special case where the 2D DFT basis is used, steps 4 and 5 can be omitted because in that case $\mathbf{G}_{m,i} = \sqrt{JD}\,\mathbf{F}_{m,i}$.

According to their definition in (28), the measurement matrices $\mathbf{\Phi}^{(s)}$ are constructed by selecting those $|\mathcal{P}^{(s)}| = Q$ rows of the scaled unitary matrix $\sqrt{\frac{JD}{Q}}\,\mathbf{U}$ that correspond to the pilot positions $\mu_q^{(s)} \in \mathcal{P}^{(s)}$. Therefore, to be consistent with the construction of measurement matrices described in Section III-A, we choose these

rows—or, in other words, the pilot positions $\mu_q^{(s)}$—uniformly at random from the subsampled grid $\mathcal{G}$. More precisely, we first choose a subset of $\mathcal{G}$ of size $N_{\mathrm{T}}Q$ uniformly at random, and then we partition it into N_{T} pairwise disjoint sets $\mathcal{P}^{(s)}$, $s \in \{1, \ldots, N_{\mathrm{T}}\}$ of equal size Q. This construction differs from the construction of measurement matrices explained in Section III-A in that here the pilot sets $\mathcal{P}^{(s)}$ (i.e. the rows of the unitary matrix $\sqrt{\frac{JD}{Q}}\,\mathbf{U}$) have to be chosen pairwise disjoint, which contradicts the assumption underlying (17) that each row of $\sqrt{\frac{JD}{Q}}\,\mathbf{U}$ is chosen with equal probability. Unfortunately, an analysis of the G-RIC for this exact scenario does not seem to exist. Nevertheless, we can expect $\mathbf{\Phi}^{(s)}$ to satisfy the group restricted isometry property with a small G-RIC with high probability (as explained in Section III-A) if the pilot sets are chosen sufficiently large.

The pilot positions are chosen and communicated to the receiver *before* the start of data transmission, and stay fixed throughout. Therefore, once pilot sets $\mathcal{P}^{(s)}$ yielding matrices $\mathbf{\Phi}^{(s)}$ with "good" MGCS reconstruction properties are found, they can be used for all future data transmissions.

C. Performance Analysis

We next derive upper bounds on the estimation error of the proposed channel estimator. Let $\mathcal{J} = \{\mathcal{I}_b\}_{b=1}^{B}$ be the partition used by the MGCS reconstruction algorithm in step 1 (the definition of $\mathcal{J}$ will be discussed in Section V). Let us denote by $\mathcal{S} \subseteq \{1, \ldots, B\}$ the set of the indices b of those S groups $\mathcal{I}_b$ that contain the effective joint support of the vectors $\mathrm{rvec}_{m,i}\{G_{m,i}^{(\theta)}\}$. Furthermore, let $\big(\mathrm{rvec}_{m,i}\{G_{m,i}^{(\theta)}\}\big)[b] \in \mathbb{C}^{|\mathcal{I}_b|}$ denote the subvector of $\mathrm{rvec}_{m,i}\{G_{m,i}^{(\theta)}\}$ comprising the entries with indices in $\mathcal{I}_b$. Then, the leakage of the vectors $\mathrm{rvec}_{m,i}\{G_{m,i}^{(\theta)}\}$ outside $\mathcal{S}$ and, thus, the error of a joint group S-sparsity assumption (i.e., the error incurred when the entries of the vectors $\mathrm{rvec}_{m,i}\{G_{m,i}^{(\theta)}\}$ outside these S groups are set to zero) can be quantified by

$$C_{G,\mathcal{S},\mathcal{J}} \triangleq \sum_{b \notin \mathcal{S}} \sqrt{\sum_{\theta \in \Theta} \big\| \big(\mathrm{rvec}_{m,i}\{G_{m,i}^{(\theta)}\}\big)[b] \big\|_2^2}\,. \tag{32}$$

We also define $C_{\mathbf{P}} \triangleq \|\mathbf{P}\|\,\|\mathbf{P}^{-1}\|$, where $\|\cdot\|$ denotes the spectral norm (i.e., the operator norm associated with the Euclidean vector norm) [67], as well as the root mean square error (RMSE) of channel estimation

$$E \triangleq \sqrt{\sum_{\theta \in \Theta} \sum_{l=0}^{L-1} \sum_{k=0}^{K-1} \big| \hat{H}_{l,k}^{(\theta)} - H_{l,k}^{(\theta)} \big|^2}\,, \tag{33}$$

with $H_{l,k}^{(\theta)} \triangleq [\mathbf{H}_{l,k}]_{r,s}$ and $\hat{H}_{l,k}^{(\theta)} \triangleq [\hat{\mathbf{H}}_{l,k}]_{r,s}$. For the following theorem, we consider the case where G-BPDN (see (13)) or G-CoSaMP (see Section III-A) is used as the MGCS reconstruction method in step 1. We assume that G-BPDN or G-CoSaMP operates in the MGCS mode described in Section III-C, so that joint sparsity and group sparsity are leveraged simultaneously. The proof of the theorem is given in Appendix A.

Theorem 1: Consider the MGCS-based channel estimator described in Section IV-B. Let $\epsilon > 0$.

1) Assume that the MGCS reconstruction method in step 1 is G-BPDN operating in MGCS mode. If all matrices $\mathbf{\Phi}^{(s)}$ in (30) satisfy the group restricted isometry property of order $2S$ with respect to $\mathcal{J}$ with G-RIC $\delta^{(s)}_{2S|\mathcal{J}} \leq \sqrt{2}-1$, and if $\sqrt{\sum_{\theta\in\Theta} \|\mathbf{z}^{(\theta)}\|_2^2} \leq \epsilon$, the channel estimation RMSE is bounded according to

$$E \leq C'_0 \frac{C_{G,\mathcal{S},\mathcal{J}}}{\sqrt{S}} + C'_1 \epsilon \,, \tag{34}$$

with the constants $C'_0 \triangleq c_0 \sqrt{\frac{KL}{JD}} C_{\mathbf{P}}$ and $C'_1 \triangleq c_1 \sqrt{\frac{KL}{Q}} \|\mathbf{P}^{-1}\|$, where c_0 and c_1 are the constants in (15).

2) Alternatively, assume that the MGCS reconstruction method in step 1 is G-CoSaMP with n iterations operating in MGCS mode. If all matrices $\mathbf{\Phi}^{(s)}$ satisfy the group restricted isometry property of order $4S$ with respect to $\mathcal{J}$ with G-RIC $\delta^{(s)}_{4S|\mathcal{J}} \leq 0.1$, and if $\sqrt{\sum_{\theta\in\Theta} \|\mathbf{z}^{(\theta)}\|_2^2} \leq \epsilon$, the channel estimation RMSE is bounded according to

$$E \leq C''_0 \Big(1 + \frac{1}{\sqrt{S}}\Big) C_{G,\mathcal{S},\mathcal{J}} + C''_1 \epsilon + C''_2(n) \,, \tag{35}$$

with the constants $C''_0 \triangleq 20\sqrt{\frac{KL}{JD}} C_{\mathbf{P}}$, $C''_1 \triangleq 20\sqrt{\frac{KL}{Q}} \|\mathbf{P}^{-1}\|$, and $C''_2(n) \triangleq \frac{1}{2^n} C_{\mathbf{P}} \times \sqrt{\frac{KL}{JD} \sum_{\theta\in\Theta} \sum_{m=0}^{D-1} \sum_{i=-J/2}^{J/2-1} \big|G^{(\theta)}_{m,i}\big|^2}$.

Note that $C''_2(n)$ can be made arbitrarily small by increasing the number n of G-CoSaMP iterations. Furthermore, note that—as mentioned at the end of Section IV-B—the matrices $\mathbf{\Phi}^{(s)}$ can be expected to satisfy the group restricted isometry property with sufficiently small G-RICs $\delta^{(s)}_{2S|\mathcal{J}}$ and $\delta^{(s)}_{4S|\mathcal{J}}$ (with high probability) if the size of the pilot sets $\mathcal{P}^{(s)}$ is chosen sufficiently large.

D. Computational Complexity

To analyze the complexity of the proposed method, we consider each step individually. The complexity of step 1 depends on the MGCS algorithm used and will be denoted as $\mathcal{O}(\mathrm{MGCS})$. The rescaling performed in step 2 requires $\mathcal{O}\big(N_{\mathrm{T}} N_{\mathrm{R}} JD\big)$ operations. The complexity of step 3 is $\mathcal{O}\big(N_{\mathrm{T}}^2 N_{\mathrm{R}} JD\big)$, because $\mathbf{P}^{-T}$ is of size $N_{\mathrm{T}} \times N_{\mathrm{T}}$, and thus each of the N_{R} matrix-vector products has complexity $\mathcal{O}\big(N_{\mathrm{T}}^2\big)$ (note that $\mathbf{P}$ has to be inverted only once before the start of data transmission). Evaluating (25) in step 4 in an entrywise (i.e., channel-by-channel) fashion requires $\mathcal{O}\big(N_{\mathrm{T}} N_{\mathrm{R}} (JD)^2\big)$ operations; a more efficient computation of (25) may be possible if the matrix $\mathbf{U}$ with columns $\mathrm{rvec}_{\lambda,\kappa}\big\{u_{m,i}[\lambda,\kappa]\big\}$ has a suitable structure. In step 5, again proceeding entrywise, the calculation of (31) can be performed efficiently in $\mathcal{O}\big(N_{\mathrm{T}} N_{\mathrm{R}} JD \log(JD)\big)$ operations by using the

FFT. By the same reasoning, step 6 has complexity $\mathcal{O}\big(N_{\mathrm{T}} N_{\mathrm{R}} KL \log(KL)\big)$. Therefore, the overall complexity of the proposed channel estimator is obtained as

$$\mathcal{O}(\text{MGCS}) + \mathcal{O}\big(N_{\mathrm{T}} N_{\mathrm{R}} (JD)^2\big) + \mathcal{O}\big(N_{\mathrm{T}} N_{\mathrm{R}} KL \log(KL)\big)\,, \tag{36}$$

since typically $N_{\mathrm{T}} \ll JD$ in practice.

Usually, the term $\mathcal{O}(\text{MGCS})$ will dominate the overall complexity. The complexity of the various MGCS algorithms depends on the implementation. For G-CoSaMP (see Section III-A), we have $\mathcal{O}(\text{MGCS}) = \mathcal{O}(\text{G-CoSaMP}) = n_{\text{G-CoSaMP}}\, \mathcal{O}(\boldsymbol{\Phi})$, where $n_{\text{G-CoSaMP}}$ is the number of G-CoSaMP iterations and $\mathcal{O}(\boldsymbol{\Phi})$ denotes the complexity of multiplying $\boldsymbol{\Phi}$ or $\boldsymbol{\Phi}^H$ by a vector of appropriate length. Taking advantage of the block-diagonal structure of $\boldsymbol{\Phi}$ (see (20) and (30)), we have $\mathcal{O}(\boldsymbol{\Phi}) \leq N_{\mathrm{R}} \sum_{s=1}^{N_{\mathrm{T}}} \mathcal{O}(\boldsymbol{\Phi}^{(s)})$ and, hence, $\mathcal{O}(\text{G-CoSaMP}) \leq n_{\text{G-CoSaMP}} N_{\mathrm{R}} \sum_{s=1}^{N_{\mathrm{T}}} \mathcal{O}(\boldsymbol{\Phi}^{(s)})$. For G-DCS-SOMP (see Section III-C), following the implementation of OMP in [68], the complexity in the special setting (30), where only N_{T} different matrices are involved, is $\mathcal{O}(\text{G-DCS-SOMP}) = n_{\text{G-DCS-SOMP}} N_{\mathrm{R}} \sum_{s=1}^{N_{\mathrm{T}}} \mathcal{O}(\boldsymbol{\Phi}^{(s)}) + \mathcal{O}\big(N_{\mathrm{T}} JD (n'_{\text{G-DCS-SOMP}})^2\big)$. Here, $n_{\text{G-DCS-SOMP}}$ denotes the number of G-DCS-SOMP iterations and $n'_{\text{G-DCS-SOMP}}$ denotes the sum of the cardinalities of the chosen groups. Finally, we note that a complexity analysis of G-BPDN does not seem to be available.

As mentioned in Section IV-B, if the 2D DFT basis is used, steps 4 and 5 can be omitted; the second term in (36) then is replaced by $\mathcal{O}(N_{\mathrm{T}}^2 N_{\mathrm{R}} JD)$ (which is due to step 3). More importantly, also the complexity of the MGCS algorithms is typically reduced, because the vector-matrix products can be calculated using FFT methods.

E. Special Case: Single-Input Single-Output Systems

We briefly consider the special case of SISO systems because of its great practical importance. In the SISO case, the vectors and matrices describing the system reduce to scalars, and (7) reduces to

$$y_\mu = H_\mu a_\mu + z_\mu\,, \tag{37}$$

with $\mu = (l, k)$. Let $\mathcal{P} \subseteq \mathcal{G}$ be a pilot set of size $|\mathcal{P}| = Q$. If we specialize the pilot scheme described in Section IV-A to the SISO setting, then the same pilot symbol p is transmitted at all time-frequency positions $\mu \in \mathcal{P}$. To allow for different pilot symbols p_μ, we modify our compressive estimator as described in the following.

For $\mu \in \mathcal{P}$, let $\tilde{y}_\mu \triangleq y_\mu / p_\mu$. Then, using (37) with $a_\mu = p_\mu$, we obtain $\tilde{y}_\mu = H_\mu + \tilde{z}_\mu$ for $\mu \in \mathcal{P}$, with $\tilde{z}_\mu \triangleq z_\mu / p_\mu$. Therefore, $\tilde{y}_\mu$ is a noisy estimate of the channel coefficient H_μ. Inserting for H_μ the expression (25), we obtain

$$\tilde{y}_\mu = \sum_{m=0}^{D-1} \sum_{i=-J/2}^{J/2-1} G_{m,i}\, u_{m,i}[\lambda,\kappa] \,+\, \tilde{z}_\mu\,, \qquad \text{for all } \mu = (\lambda\Delta L, \kappa\Delta K) \in \mathcal{P}. \tag{38}$$

To rewrite this in vector-matrix notation, we define $\mathbf{U}$ as in Section IV-B, and we set $\mathbf{\Phi} \triangleq \sqrt{\frac{JD}{Q}}\tilde{\mathbf{U}}$, where $\tilde{\mathbf{U}}$ is the $Q \times JD$ submatrix of $\mathbf{U}$ constituted by the Q rows corresponding to the pilot positions $\mu_q \in \mathcal{P}$, with $q \in \{1,\dots,Q\}$. Furthermore, let $\tilde{\mathbf{x}} \triangleq \sqrt{\frac{Q}{JD}}\,\mathrm{rvec}_{m,i}\{G_{m,i}\} \in \mathbb{C}^{JD}$, $\tilde{\mathbf{y}} \triangleq (\tilde{y}_{\mu_1} \cdots \tilde{y}_{\mu_Q})^T$, and $\tilde{\mathbf{z}} \triangleq (\tilde{z}_{\mu_1} \cdots \tilde{z}_{\mu_Q})^T$. We can then write (38) as

$$\tilde{\mathbf{y}} = \mathbf{\Phi}\tilde{\mathbf{x}} + \tilde{\mathbf{z}}\,. \tag{39}$$

This is a measurement equation of the form (12), of dimension $Q \times JD$. In practice, $Q \ll JD$. Since the coefficients $G_{m,i}$ are assumed (approximately) group sparse, the vector $\tilde{\mathbf{x}}$ is (approximately) group sparse, and therefore any GCS reconstruction algorithm as discussed in Section III-A can be used to reconstruct $\tilde{\mathbf{x}}$. The resulting channel estimation algorithm can then be stated as follows:

1) Stack the preliminary channel estimates at the pilot positions, $\tilde{y}_{\mu_q}$, into the vector $\tilde{\mathbf{y}}$ as described above, and use a GCS reconstruction algorithm to obtain an estimate $\hat{\tilde{\mathbf{x}}}$ of $\tilde{\mathbf{x}}$.
2) Rescale $\hat{\tilde{\mathbf{x}}}$ with $\sqrt{\frac{JD}{Q}}$ to obtain an estimate of $G_{m,i}$, i.e., calculate $\mathrm{rvec}_{m,i}\{\hat{G}_{m,i}\} = \sqrt{\frac{JD}{Q}}\hat{\tilde{\mathbf{x}}}$.
3) From $\hat{G}_{m,i}$, calculate estimates $\hat{H}_{\lambda\,\Delta L,\kappa\,\Delta K}$ of the subsampled channel coefficients $H_{\lambda\,\Delta L,\kappa\,\Delta K}$ according to (25), i.e., $\hat{H}_{\lambda\,\Delta L,\kappa\,\Delta K} = \sum_{m=0}^{D-1}\sum_{i=-J/2}^{J/2-1} \hat{G}_{m,i}\, u_{m,i}[\lambda,\kappa]$.
4) Calculate estimated 2D DFT coefficients $\hat{F}_{m,i}$ according to the inversion of (24), i.e.,

$$\hat{F}_{m,i} \;=\; \begin{cases} \dfrac{1}{JD}\displaystyle\sum_{\lambda=0}^{J-1}\sum_{\kappa=0}^{D-1} \hat{H}_{\lambda\,\Delta L,\kappa\,\Delta K}\, e^{-j2\pi(\frac{i\lambda}{J}-\frac{m\kappa}{D})}, & m \in \{0,\dots,D-1\},\, i \in \{-J/2,\dots,J/2-1\} \\ 0\,, & \text{otherwise.} \end{cases}$$

5) Calculate estimates of all channels coefficients $H_{l,k}$ by using (10), i.e., $\hat{H}_{l,k} = \sum_{m=0}^{K-1}\sum_{i=-L/2}^{L/2-1} \hat{F}_{m,i}\, e^{-j2\pi(\frac{km}{K}-\frac{li}{L})}$.

Again, steps 3 and 4 can be omitted if the 2D DFT basis is used, because then $G_{m,i} = \sqrt{JD}\,F_{m,i}$. The pilot positions μ_q have to be chosen uniformly at random from the subsampled grid $\mathcal{G}$ in order to be consistent with the construction of measurement matrices described in Section III-A. They are chosen and communicated to the receiver before the start of data transmission.

For a bound on the channel estimation error, let $\mathcal{J} = \{\mathcal{I}_b\}_{b=1}^{B}$ denote the partition used by the GCS reconstruction algorithm in step 1, and let $\mathcal{S} \subseteq \{1,\dots,B\}$ denote the set of the indices b of those S groups $\mathcal{I}_b$ that contain the effective support of the vector $\mathrm{rvec}_{m,i}\{G_{m,i}\}$. Similarly to Section IV-C, we measure the leakage of $\mathrm{rvec}_{m,i}\{G_{m,i}\}$ outside $\mathcal{S}$ by $C_{G,S,\mathcal{J}} \triangleq \sum_{b\notin\mathcal{S}} \big\|\big(\mathrm{rvec}_{m,i}\{G_{m,i}\}\big)[b]\big\|_2$. We can then specialize

Theorem 1 as follows. If the GCS reconstruction method in step 1 is G-BPDN, if $\mathbf{\Phi}$ satisfies the group restricted isometry property of order $2S$ with respect to $\mathcal{J}$ with G-RIC $\delta_{2S|\mathcal{J}} \leq \sqrt{2}-1$, and if $\|\tilde{\mathbf{z}}\|_2 \leq \epsilon$, the channel estimation RMSE $E \triangleq \sqrt{\sum_{l=0}^{L-1}\sum_{k=0}^{K-1}\left|\hat{H}_{l,k}-H_{l,k}\right|^2}$ is bounded according to

$$E \leq C_0' \frac{C_{G,S,\mathcal{J}}}{\sqrt{S}} + C_1' \epsilon \,,$$

with $C_0' \triangleq c_0\sqrt{\frac{KL}{JD}}$ and $C_1' \triangleq c_1\sqrt{\frac{KL}{Q}}$, where c_0 and c_1 are the constants in (15). Similarly, if the GCS reconstruction method in step 1 is G-CoSaMP with n iterations, if $\mathbf{\Phi}$ satisfies the group restricted isometry property of order $4S$ with respect to $\mathcal{J}$ with G-RIC $\delta_{4S|\mathcal{J}} \leq 0.1$, and if $\|\tilde{\mathbf{z}}\|_2 \leq \epsilon$, then

$$E \leq C_0''\Big(1+\frac{1}{\sqrt{S}}\Big) C_{G,S,\mathcal{J}} + C_1''\epsilon + C_2''(n) \,,$$

with $C_0'' \triangleq 20\sqrt{\frac{KL}{JD}}$, $C_1'' \triangleq 20\sqrt{\frac{KL}{Q}}$, and $C_2''(n) \triangleq \frac{1}{2^n}\sqrt{\frac{KL}{JD}\sum_{m=0}^{D-1}\sum_{i=-J/2}^{J/2-1}|G_{m,i}|^2}$. As in the MIMO case, for both bounds, the respective condition on the G-RIC can be met (with high probability) by choosing a sufficiently large pilot set $\mathcal{P}$. A sufficient condition is provided by (17).

The analysis of the complexity in the SISO case closely follows that of the general MIMO case in Section IV-D. The complexity of step 1 depends on the GCS algorithm used and will be denoted by $\mathcal{O}(\text{GCS})$. The complexities of steps 2–5 are $\mathcal{O}(JD)$, $\mathcal{O}\big((JD)^2\big)$, $\mathcal{O}\big(JD\log(JD)\big)$, and $\mathcal{O}\big(KL\log(KL)\big)$, respectively. Thus, the overall complexity of the proposed channel estimator is

$$\mathcal{O}(\text{GCS}) + \mathcal{O}\big((JD)^2\big) + \mathcal{O}\big(KL\log(KL)\big) \,,$$

which is a special case of (36). If the 2D DFT basis is used, steps 3 and 4 can be omitted and the overall complexity becomes $\mathcal{O}(\text{GCS}) + \mathcal{O}\big(KL\log(KL)\big)$. If the GCS algorithm is G-CoSaMP, then $\mathcal{O}(\text{GCS}) = \mathcal{O}(\text{G-CoSaMP}) = n_{\text{G-CoSaMP}}\,\mathcal{O}(\mathbf{\Phi})$, where $n_{\text{G-CoSaMP}}$ and $\mathcal{O}(\mathbf{\Phi})$ are defined as before. If the GCS algorithm is G-OMP, then $\mathcal{O}(\text{GCS}) = \mathcal{O}(\text{G-OMP}) = \mathcal{O}(n_{\text{G-OMP}}QJD)$, where $n_{\text{G-OMP}}$ denotes the number of OMP iterations.

Finally, we note that if the group size in partition $\mathcal{J}$ is reduced to the smallest possible value 1, so that each group $\mathcal{I}_b$ contains only a single index j, the proposed method reduces to the compressive SISO channel estimator presented in [26]. At the other extreme, if the largest possible group size JD is chosen, so that there is only a single group containing all indices $j \in \{1,\ldots,JD\}$, then using G-OMP in step 1 reduces to conventional least squares reconstruction.

V. Joint Group Sparsity in the Delay-Doppler Domain

In this section, we analyze the joint group sparsity of the 2D DFT expansion coefficients $F_{m,i}^{(\theta)}$, $\theta \in \Theta$ (see (10) and (11)). More precisely, we will demonstrate that the JD-dimensional vectors $\mathrm{rvec}_{m,i}\{F_{m,i}^{(\theta)}\}$, $\theta \in \Theta$, which are obtained by rowwise stacking of the $D \times J$ "matrices" $F_{m,i}^{(\theta)}$, are approximately jointly group sparse with respect to some partition $\mathcal{J}$. This partition will be explicitly specified in Section V-C. However, we will first discuss the special cases of group sparsity and joint sparsity in Sections V-A and V-B, respectively. For this discussion, we will omit the matrix-to-vector stacking operations and thus deal directly with 2D functions, using suitably adapted sparsity notions.

Because of (11), analyzing the joint group sparsity of the $F_{m,i}^{(\theta)}$, $\theta \in \Theta$ basically amounts to studying the joint group sparsity of the spreading functions $S_h^{(\theta)}[m,i]$. Indeed, (11) written entrywise reads

$$F_{m,i}^{(\theta)} \;=\; \sum_{q=0}^{N-1} S_h^{(\theta)}[m, i+qL]\, A_{\gamma,g}^{*}\!\left(m, \frac{i+qL}{L_{\mathrm{r}}}\right), \tag{40}$$

and neither the multiplication by $A_{\gamma,g}^{*}\big(m, \frac{i+qL}{L_{\mathrm{r}}}\big)$ nor the summation with respect to q can create any "new" nonzeros. To study the joint group sparsity of the $S_h^{(\theta)}[m,i]$, we will assume that each channel comprises P propagation paths (multipath components) corresponding to the same set of P specular scatterers with channel-dependent delays $\tau_p^{(\theta)}$ and Doppler frequency shifts $\nu_p^{(\theta)}$, for $p = 1, \ldots, P$. Thus, the channel impulse responses can be written as

$$h^{(\theta)}(t,\tau) \;=\; \sum_{p=1}^{P} \eta_p^{(\theta)}\, \delta\big(\tau - \tau_p^{(\theta)}\big)\, e^{j2\pi\nu_p^{(\theta)} t}, \qquad \theta \in \Theta\,, \tag{41}$$

where the $\eta_p^{(\theta)}$ are complex path gains. This model is often a good approximation of real mobile radio channels [69–71]. We emphasize that we use it only for analyzing the sparsity structure of the $F_{m,i}^{(\theta)}$ and for motivating the basis optimization in Section VI; it is not required for the proposed channel estimation methods.

For the model (41), the discrete-delay-Doppler spreading functions (9) are obtained as

$$S_h^{(\theta)}[m,i] \;=\; \sum_{p=1}^{P} \eta_p^{(\theta)}\, e^{j\pi\left(\nu_p^{(\theta)} T_{\mathrm{s}} - \frac{i}{L_{\mathrm{r}}}\right)(L_{\mathrm{r}}-1)}\, \Lambda_p^{(\theta)}[m,i]\,, \tag{42}$$

with the *shifted leakage kernels*

$$\Lambda_p^{(\theta)}[m,i] \;\triangleq\; \phi^{(\nu_p^{(\theta)})}\!\left(m - \frac{\tau_p^{(\theta)}}{T_{\mathrm{s}}}\right) \psi\big(i - \nu_p^{(\theta)} T_{\mathrm{s}} L_{\mathrm{r}}\big)\,, \tag{43}$$

where $\phi^{(\nu)}(x) \triangleq \int_{-\infty}^{\infty} f_1(T_{\mathrm{s}}x - t)\, f_2(t)\, e^{-j2\pi\nu t} dt$ and $\psi(x) \triangleq \sin(\pi x)/\big(L_{\mathrm{r}} \sin(\pi x / L_{\mathrm{r}})\big)$. In [26], it is shown that each $\Lambda_p^{(\theta)}[m,i]$ is effectively supported in a rectangular region of some delay length $\Delta\widetilde{m} \in \mathbb{N}$ and Doppler length $\Delta\widetilde{i} \in \mathbb{N}$, centered about the delay-Doppler point $\zeta_p^{(\theta)} \triangleq \big(\tau_p^{(\theta)}/T_{\mathrm{s}}, \nu_p^{(\theta)} T_{\mathrm{s}} L_{\mathrm{r}}\big)$. Therefore, each $\Lambda_p^{(\theta)}[m,i]$ is

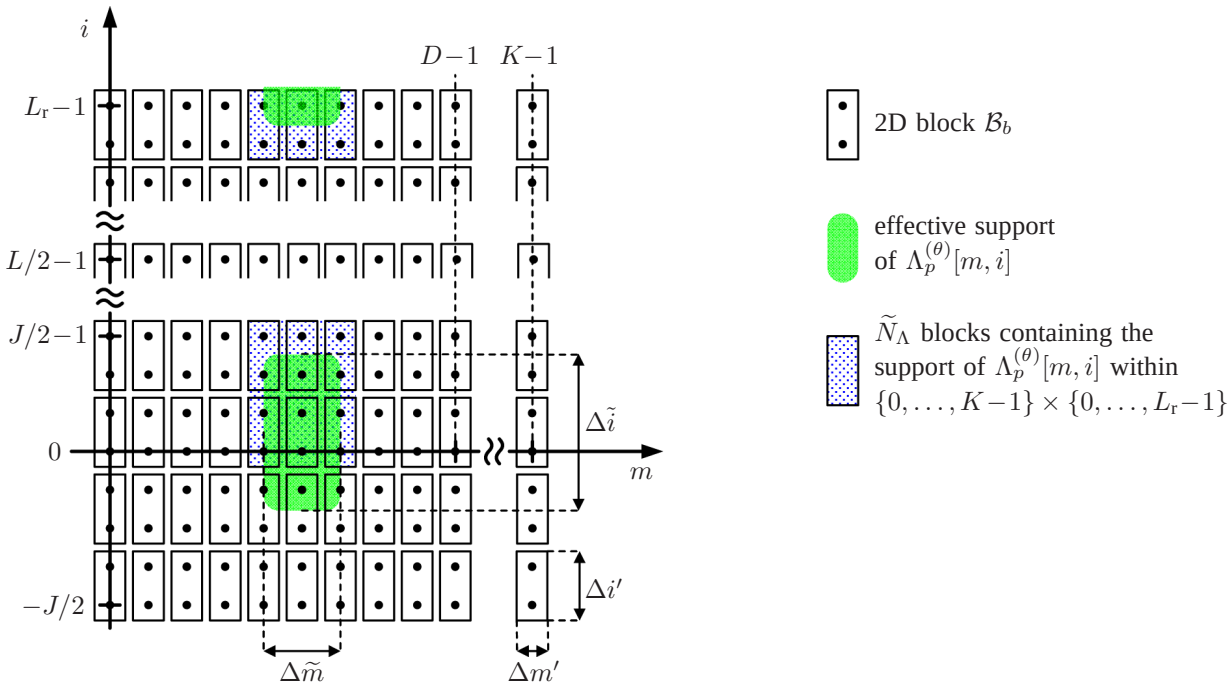

Fig. 2. Illustration of the 2D block tiling $\{\mathcal{B}_b\}$, the effective support of a shifted leakage kernel $\Lambda_p^{(\theta)}[m,i]$, and the $\widetilde{N}_\Lambda$ blocks containing this effective support. In this example, $\Delta\widetilde{m}=2$, $\Delta\tilde{i}=4$, $\Delta m'=1$, $\Delta i'=2$, and $\widetilde{N}_\Lambda=9$.

approximately $\Delta\widetilde{m}\Delta\tilde{i}$-sparse. Here, $\Delta\widetilde{m}$ and $\Delta\tilde{i}$ can be chosen such that a prescribed approximation quality is achieved. Typically, $\Delta\widetilde{m}$ can be chosen quite small because the functions $\phi^{(\nu)}(x)$ decay rather rapidly, whereas $\Delta\tilde{i}$ has to be chosen larger because $\psi(x)$ decays more slowly.

A. Group Sparsity

We first analyze the group sparsity of $F_{m,i}^{(\theta)}$ for a single (arbitrary but fixed) θ. Consider a tiling of $\mathbb{Z}\times\mathbb{Z}$ into 2D blocks $\mathcal{B}_b$ of equal size $\Delta m'\times\Delta i'$, where $\Delta m'$ divides D, $\Delta i'$ divides $J/2$, and $\{0,\dots,\Delta m'-1\}\times\{0,\dots,\Delta i'-1\}$ is one of these blocks. Such a tiling is depicted in Figure 2. As visualized in the figure, the effective support of each shifted leakage kernel $\Lambda_p^{(\theta)}[m,i]$ within $\{0,\dots,K-1\}\times\{0,\dots,L_{\mathrm{r}}-1\}$ is contained in at most $\widetilde{N}_\Lambda$ blocks $\mathcal{B}_b$, where

$$\widetilde{N}_\Lambda \triangleq \left(\left\lceil\frac{\Delta\widetilde{m}}{\Delta m'}\right\rceil+1\right)\left(\left\lceil\frac{\Delta\tilde{i}}{\Delta i'}\right\rceil+1\right). \tag{44}$$

Thus, because of (42), the support of $S_h^{(\theta)}[m,i]$ is contained in at most $P\widetilde{N}_\Lambda$ blocks. Since $\Delta i'$ divides L (because $\Delta i'$ divides $J/2$ and J divides L), the summation in (40) only adds up whole blocks. Therefore, the nonzeros contained in a single block cannot be spread over several blocks by the summation and thus no "new" nonzero blocks within the fundamental region $\{0,\dots,D-1\}\times\{-J/2,\dots,J/2-1\}$ can be created. Also, since

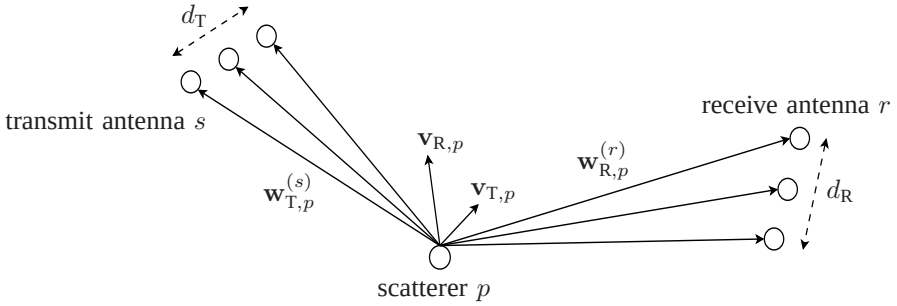

Fig. 3. Illustration of the propagation path from transmit antenna s to receive antenna r via scatterer p in a 3×3 MIMO system.

$\Delta m'$ divides D and $\Delta i'$ divides $J/2$, the support restriction of $F_{m,i}^{(\theta)}$ to $\{0,\dots,D-1\}\times\{-J/2,\dots,J/2-1\}$ is compatible with the block boundaries (note that $S_h^{(\theta)}[m,i]$ is L_{r}-periodic in i). Thus, the effective support of $F_{m,i}^{(\theta)}$ within $\{0,\dots,D-1\}\times\{-J/2,\dots,J/2-1\}$ is contained in at most $P\widetilde{N}_\Lambda$ blocks. Therefore, $F_{m,i}^{(\theta)}$ can be considered approximately group $P\widetilde{N}_\Lambda$-sparse with respect to the tiling $\{\mathcal{B}_b\}$.

B. Joint Sparsity

Next, we analyze the joint sparsity of the $F_{m,i}^{(\theta)}$, $\theta\in\Theta$. We first consider the shifted leakage kernels $\Lambda_p^{(\theta_1)}[m,i]$ and $\Lambda_p^{(\theta_2)}[m,i]$ of two different channels $\theta_1=(r_1,s_1)$ and $\theta_2=(r_2,s_2)$, corresponding to the same scatterer p. As mentioned in Section V-A, these leakage kernels are effectively supported in rectangular regions of equal size $\Delta\widetilde{m}\times\Delta\tilde{i}$ that are centered about $\zeta_p^{(\theta_1)}=\big(\tau_p^{(\theta_1)}/T_{\mathrm{s}},\nu_p^{(\theta_1)}T_{\mathrm{s}}L_{\mathrm{r}}\big)$ and $\zeta_p^{(\theta_2)}=\big(\tau_p^{(\theta_2)}/T_{\mathrm{s}},\nu_p^{(\theta_2)}T_{\mathrm{s}}L_{\mathrm{r}}\big)$. We will show that, typically, these center points are very close to each other, and therefore the supports of the two leakage kernels strongly overlap.

Time delay. Consider the transmit antennas, the receive antennas, and an arbitrary scatterer p, as depicted in Figure 3. Let $\mathbf{w}_{\mathrm{T},p}^{(s)}$ and $\mathbf{w}_{\mathrm{R},p}^{(r)}$ denote the vectors connecting scatterer p with transmit antenna s and receive antenna r, respectively, and let $w_{\mathrm{T},p}^{(s)}\triangleq\big\|\mathbf{w}_{\mathrm{T},p}^{(s)}\big\|_2$ and $w_{\mathrm{R},p}^{(r)}\triangleq\big\|\mathbf{w}_{\mathrm{R},p}^{(r)}\big\|_2$. The time delay $\tau_p^{(\theta)}$ for scatterer p and antenna pair $\theta=(r,s)$ is then obtained as

$$\tau_p^{(\theta)}=\frac{w_{\mathrm{T},p}^{(s)}+w_{\mathrm{R},p}^{(r)}}{c}\,, \tag{45}$$

where c denotes the speed of light. We can bound the difference between the time delays of two different channels θ_1 and θ_2, $\Delta\tau_p^{(\theta_1,\theta_2)}\triangleq\big|\tau_p^{(\theta_1)}-\tau_p^{(\theta_2)}\big|$, as follows. Using (45), we have

$$\Delta\tau_p^{(\theta_1,\theta_2)}\;=\;\frac{1}{c}\big|w_{\mathrm{T},p}^{(s_1)}+w_{\mathrm{R},p}^{(r_1)}-w_{\mathrm{T},p}^{(s_2)}-w_{\mathrm{R},p}^{(r_2)}\big|\;\le\;\frac{1}{c}\big(\big|w_{\mathrm{T},p}^{(s_1)}-w_{\mathrm{T},p}^{(s_2)}\big|+\big|w_{\mathrm{R},p}^{(r_1)}-w_{\mathrm{R},p}^{(r_2)}\big|\big)\,. \tag{46}$$

It follows from elementary geometric considerations that the difference between the transmitter-scatterer path lengths, $\big|w_{\mathrm{T},p}^{(s_1)}-w_{\mathrm{T},p}^{(s_2)}\big|$, cannot be larger than the distance between the two transmit antennas s_1 and s_2. This

distance, in turn, is bounded by the maximum distance between any two transmit antennas, which will be denoted by d_{T}. Thus, $\left|w_{\mathrm{T},p}^{(s_1)} - w_{\mathrm{T},p}^{(s_2)}\right| \leq d_{\mathrm{T}}$. Using the same argument for the scatterer-receiver path, we obtain $\left|w_{\mathrm{R},p}^{(r_1)} - w_{\mathrm{R},p}^{(r_2)}\right| \leq d_{\mathrm{R}}$, where d_{R} denotes the maximum distance between any two receive antennas. Inserting these bounds into (46), we obtain the bound

$$\Delta\tau_p^{(\theta_1,\theta_2)} \leq \tau_{\mathrm{B}}\,, \quad \text{with } \tau_{\mathrm{B}} \triangleq \frac{d_{\mathrm{T}} + d_{\mathrm{R}}}{c}\,. \tag{47}$$

Doppler frequency shift. Next, we consider the Doppler frequency shift $\nu_p^{(\theta)}$ for scatterer p and antenna pair $\theta = (r, s)$. If the source of a sinusoidal electromagnetic wave with frequency f_0 moves towards an observer with relative velocity v, at an angle α relative to the direction from the observer to the source, the Doppler frequency shift is approximately given by[3] $\nu = f_0 \frac{v}{c} \cos\alpha$ [72]. In our case, because transmitter, receiver, and scatterers are moving, the Doppler effect occurs twice. Let $\mathbf{v}_{\mathrm{T},p}$ and $\mathbf{v}_{\mathrm{R},p}$ denote the velocity vectors of scatterer p relative to transmitter and receiver, respectively, and let $v_{\mathrm{T},p} \triangleq \|\mathbf{v}_{\mathrm{T},p}\|_2$ and $v_{\mathrm{R},p} \triangleq \|\mathbf{v}_{\mathrm{R},p}\|_2$. First, we consider the transmission from antenna s to scatterer p, with carrier (center) frequency f_0. Let α denote the angle between $\mathbf{v}_{\mathrm{T},p}$ and $\mathbf{w}_{\mathrm{T},p}^{(s)}$, and note that $\cos\alpha = \frac{\mathbf{v}_{\mathrm{T},p}^T \mathbf{w}_{\mathrm{T},p}^{(s)}}{v_{\mathrm{T},p} w_{\mathrm{T},p}^{(s)}}$. The carrier frequency observed at scatterer p is approximately $f_1 = f_0 + \nu_{\mathrm{T},p}^{(s)}$, with the Doppler frequency shift

$$\nu_{\mathrm{T},p}^{(s)} \;=\; f_0 \,\frac{v_{\mathrm{T},p}}{c}\cos\alpha \;=\; f_0 \,\frac{v_{\mathrm{T},p}}{c}\,\frac{\mathbf{v}_{\mathrm{T},p}^T \mathbf{w}_{\mathrm{T},p}^{(s)}}{v_{\mathrm{T},p} w_{\mathrm{T},p}^{(s)}} \;=\; \frac{f_0}{c}\,\frac{\mathbf{v}_{\mathrm{T},p}^T \mathbf{w}_{\mathrm{T},p}^{(s)}}{w_{\mathrm{T},p}^{(s)}}\,. \tag{48}$$

Next, we consider the transmission from scatterer p to receive antenna r, with carrier (center) frequency f_1. The observed carrier frequency at receive antenna r is given by $f_2 = f_1 + \nu_{\mathrm{R},p}^{(r)}$, with the Doppler frequency shift (cf. (48))

$$\nu_{\mathrm{R},p}^{(r)} \;=\; \frac{f_1}{c}\,\frac{\mathbf{v}_{\mathrm{R},p}^T \mathbf{w}_{\mathrm{R},p}^{(r)}}{w_{\mathrm{R},p}^{(r)}}\,. \tag{49}$$

By inserting for f_1, we further obtain $f_2 = f_0 + \nu_{\mathrm{T},p}^{(s)} + \nu_{\mathrm{R},p}^{(r)}$, which yields the overall Doppler frequency shift as

$$\nu_p^{(\theta)} \;=\; \nu_{\mathrm{T},p}^{(s)} + \nu_{\mathrm{R},p}^{(r)}\,. \tag{50}$$

We can now bound the difference between the Doppler frequency shifts of two different channels θ_1 and θ_2, $\Delta\nu_p^{(\theta_1,\theta_2)} \triangleq \left|\nu_p^{(\theta_1)} - \nu_p^{(\theta_2)}\right|$, as follows. Using (50), we have

$$\Delta\nu_p^{(\theta_1,\theta_2)} \;=\; \left|\nu_{\mathrm{T},p}^{(s_1)} + \nu_{\mathrm{R},p}^{(r_1)} - \nu_{\mathrm{T},p}^{(s_2)} - \nu_{\mathrm{R},p}^{(r_2)}\right| \;\leq\; \left|\nu_{\mathrm{T},p}^{(s_1)} - \nu_{\mathrm{T},p}^{(s_2)}\right| + \left|\nu_{\mathrm{R},p}^{(r_1)} - \nu_{\mathrm{R},p}^{(r_2)}\right|. \tag{51}$$

[3]Note that we do not take into account rotations of the transmitter and/or the receiver, which would yield different velocity vectors for different transmit/receive antennas. Although such rotations could be easily included in the analysis, we choose to ignore them for simplicity of exposition and because the differences of the velocity vectors are typically small.

For the transmitter-scatterer path, we obtain using (48)

$$\begin{aligned}\left|\nu_{\mathrm{T},p}^{(s_1)}-\nu_{\mathrm{T},p}^{(s_2)}\right| &= \frac{f_0}{c}\left|\mathbf{v}_{\mathrm{T},p}^{T}\left(\frac{\mathbf{w}_{\mathrm{T},p}^{(s_1)}}{w_{\mathrm{T},p}^{(s_1)}}-\frac{\mathbf{w}_{\mathrm{T},p}^{(s_2)}}{w_{\mathrm{T},p}^{(s_2)}}\right)\right| \\ &\overset{(a)}{\leq} \frac{f_0}{c}\,v_{\mathrm{T},p}\left\|\frac{\mathbf{w}_{\mathrm{T},p}^{(s_1)}}{w_{\mathrm{T},p}^{(s_1)}}-\frac{\mathbf{w}_{\mathrm{T},p}^{(s_2)}}{w_{\mathrm{T},p}^{(s_2)}}\right\|_2 \\ &\overset{(b)}{\leq} \frac{f_0}{c}\,v_{\mathrm{T},p}\,\frac{\left\|\mathbf{w}_{\mathrm{T},p}^{(s_1)}-\mathbf{w}_{\mathrm{T},p}^{(s_2)}\right\|_2}{w_{\mathrm{T},p,\min}^{(s_1,s_2)}} \\ &\overset{(c)}{\leq} \frac{f_0}{c}\,\frac{v_{\mathrm{T},p}\,d_{\mathrm{T}}}{w_{\mathrm{T},p,\min}^{(s_1,s_2)}}\,,\end{aligned}$$

with $w_{\mathrm{T},p,\min}^{(s_1,s_2)} \triangleq \min\left\{w_{\mathrm{T},p}^{(s_1)}, w_{\mathrm{T},p}^{(s_2)}\right\}$. Here, (a) is due to the Cauchy-Schwarz inequality, (b) follows from the inequality

$$\left\|\frac{\mathbf{a}}{\|\mathbf{a}\|_2}-\frac{\mathbf{b}}{\|\mathbf{b}\|_2}\right\|_2 \leq \frac{\|\mathbf{a}-\mathbf{b}\|_2}{\min\{\|\mathbf{a}\|_2\,,\|\mathbf{b}\|_2\}}\,, \tag{52}$$

which is proven in Appendix B, and (c) is a consequence of $\left\|\mathbf{w}_{\mathrm{T},p}^{(s_1)}-\mathbf{w}_{\mathrm{T},p}^{(s_2)}\right\|_2 \leq d_{\mathrm{T}}$. Based on (49), a similar derivation for the scatterer-receiver path yields $\left|\nu_{\mathrm{R},p}^{(r_1)}-\nu_{\mathrm{R},p}^{(r_2)}\right| \leq \frac{f_1}{c}\frac{v_{\mathrm{R},p}\,d_{\mathrm{R}}}{w_{\mathrm{R},p,\min}^{(r_1,r_2)}}$, where $w_{\mathrm{R},p,\min}^{(r_1,r_2)} \triangleq \min\left\{w_{\mathrm{R},p}^{(r_1)}, w_{\mathrm{R},p}^{(r_2)}\right\}$. Inserting these bounds into (51), we obtain

$$\Delta\nu_p^{(\theta_1,\theta_2)} \leq \nu_{\mathrm{B},p}^{(\theta_1,\theta_2)}, \quad \text{with } \nu_{\mathrm{B},p}^{(\theta_1,\theta_2)} \triangleq \frac{1}{c}\left(\frac{f_0\,v_{\mathrm{T},p}\,d_{\mathrm{T}}}{w_{\mathrm{T},p,\min}^{(s_1,s_2)}}+\frac{f_1 v_{\mathrm{R},p}\,d_{\mathrm{R}}}{w_{\mathrm{R},p,\min}^{(r_1,r_2)}}\right). \tag{53}$$

Joint sparsity of the coefficient functions $F_{m,i}^{(\theta)}$. From the bound (47) on $\Delta\tau_p^{(\theta_1,\theta_2)}$ and the bound (53) on $\Delta\nu_p^{(\theta_1,\theta_2)}$, it follows that the center points $\zeta_p^{(\theta_1)} = \left(\tau_p^{(\theta_1)}/T_{\mathrm{s}}, \nu_p^{(\theta_1)}T_{\mathrm{s}}L_{\mathrm{r}}\right)$ and $\zeta_p^{(\theta_2)} = \left(\tau_p^{(\theta_2)}/T_{\mathrm{s}}, \nu_p^{(\theta_2)}T_{\mathrm{s}}L_{\mathrm{r}}\right)$ of the shifted leakage kernels $\Lambda_p^{(\theta_1)}[m,i]$ and $\Lambda_p^{(\theta_2)}[m,i]$ differ by at most $\tau_{\mathrm{B}}/T_{\mathrm{s}}$ in the m-direction and by at most $\nu_{\mathrm{B},p}^{(\theta_1,\theta_2)}T_{\mathrm{s}}L_{\mathrm{r}}$ in the i-direction. Since this is true for *any* pair of channels θ_1 and θ_2, we can conclude that all $\Lambda_p^{(\theta)}[m,i]$, $\theta \in \Theta$ are (approximately) jointly $\Delta m\Delta i$-sparse, where

$$\Delta m \triangleq \Delta\widetilde{m} + \lceil \tau_{\mathrm{B}}/T_{\mathrm{s}} \rceil \quad \text{and} \quad \Delta i \triangleq \Delta\tilde{i} + \lceil \nu_{\mathrm{B}}T_{\mathrm{s}}L_{\mathrm{r}} \rceil\,,$$

with $\nu_{\mathrm{B}} \triangleq \max_{p,\theta_1\neq\theta_2}\left\{\nu_{\mathrm{B},p}^{(\theta_1,\theta_2)}\right\}$. (Here, we used the fact that the effective supports of $\Lambda_p^{(\theta_1)}[m,i]$ and $\Lambda_p^{(\theta_2)}[m,i]$ have size $\Delta\widetilde{m}\times\Delta\tilde{i}$.) With (42), it then follows that the spreading functions $S_h^{(\theta)}[m,i]$ are (approximately) jointly $P\Delta m\Delta i$-sparse. Finally, because of (40), the same is true for the $F_{m,i}^{(\theta)}$ (as discussed before).

Since the antenna spacings are typically much smaller than the path lengths, i.e., $d_{\mathrm{T}} \ll w_{\mathrm{T},p}^{(s)}$ and $d_{\mathrm{R}} \ll w_{\mathrm{R},p}^{(r)}$, and for practically relevant velocities $v_{\mathrm{T},p}$ and $v_{\mathrm{R},p}$, $\lceil\tau_{\mathrm{B}}/T_{\mathrm{s}}\rceil$ and $\lceil\nu_{\mathrm{B}}T_{\mathrm{s}}L_{\mathrm{r}}\rceil$ will be small compared to $\Delta\widetilde{m}$ and

$\Delta\tilde{i}$, respectively. Therefore, the *joint* sparsity order $P\Delta m\Delta i = P\big(\Delta\widetilde{m} + \lceil \tau_{\mathrm{B}}/T_{\mathrm{s}} \rceil\big)\big(\Delta\tilde{i} + \lceil \nu_{\mathrm{B}} T_{\mathrm{s}} L_{\mathrm{r}} \rceil\big)$ will not be much larger than the *individual* sparsity orders $P\Delta\widetilde{m}\Delta\tilde{i}$ of the coefficient functions $F_{m,i}^{(\theta)}$.

C. Joint Group Sparsity

We reconsider the tiling of $\mathbb{Z}\times\mathbb{Z}$ into the 2D blocks $\mathcal{B}_b$ as previously considered in Section V-A, restricting it to $\{0,\dots,D-1\} \times \{-J/2,\dots,J/2-1\}$ (see Figure 2). Within this region, we obtain a finite number B of blocks $\mathcal{B}_b$, $b \in \{1,\dots,B\}$. We recall that the blocks are of equal size $|\mathcal{B}_b| = \Delta m'\Delta i'$, and hence $B = \frac{JD}{\Delta m'\Delta i'}$. Since the leakage kernels $\Lambda_p^{(\theta)}[m,i]$, $\theta \in \Theta$ are (approximately) jointly $\Delta m\Delta i$-sparse, as we just showed in Section V-B, it follows by the same reasoning as in Section V-A that their effective supports are jointly contained in at most N_Λ blocks $\mathcal{B}_b$, where (cf. (44))

$$N_\Lambda \triangleq \left(\left\lceil \frac{\Delta m}{\Delta m'} \right\rceil + 1\right)\left(\left\lceil \frac{\Delta i}{\Delta i'} \right\rceil + 1\right).$$

Thus, again following (42) and (11), the $F_{m,i}^{(\theta)}$, $\theta \in \Theta$ are (approximately) jointly group PN_Λ-sparse with respect to the tiling $\{\mathcal{B}_b\}_{b=1}^{B}$.

This joint group sparsity of the $F_{m,i}^{(\theta)}$ translates into a joint group sparsity of the vectors $\mathrm{rvec}_{m,i}\{F_{m,i}^{(\theta)}\}$, $\theta \in \Theta$ that are obtained by a rowwise stacking of the $D\times J$ "matrices" $F_{m,i}^{(\theta)}$ into JD-dimensional vectors. The stacking operator $\mathrm{rvec}_{m,i}\{\cdot\}$ corresponds to the one-to-one 2D $\to$ 1D index mapping

$$\mathsf{S}\colon \{0,\dots,D-1\} \times \{-J/2,\dots,J/2-1\} \to \{1,\dots,JD\}, \qquad \mathsf{S}(m,i) \triangleq mJ + i + J/2 + 1\,. \tag{54}$$

Under this index mapping, the 2D blocks $\mathcal{B}_b$ are converted into the 1D *groups* $\mathcal{I}_b \triangleq \mathsf{S}(\mathcal{B}_b) \subseteq \{1,\dots,JD\}$, $b \in \{1,\dots,B\}$, which are of equal size $|\mathcal{I}_b| = |\mathcal{B}_b| = \Delta m'\Delta i'$. Clearly, $\mathcal{J} \triangleq \{\mathcal{I}_b\}_{b=1}^{B}$ constitutes a partition of $\{1,\dots,JD\}$, as required by the definition of joint group sparsity in Section III-C. Then, because the effective supports of all the $F_{m,i}^{(\theta)}$ within $\{0,\dots,D-1\} \times \{-J/2,\dots,J/2-1\}$ are jointly contained in at most PN_Λ blocks $\mathcal{B}_b$, it follows that the vectors $\mathrm{rvec}_{m,i}\{F_{m,i}^{(\theta)}\}$ are (approximately) jointly group PN_Λ-sparse with respect to the 1D partition $\mathcal{J}$.

VI. Basis Optimization

In this section, we propose a framework and an algorithm for optimizing the orthonormal 2D basis $\{u_{m,i}[\lambda,\kappa]\}$. Our goal is to maximize the joint group sparsity of the coefficients $G_{m,i}^{(\theta)}$ defined by the expansion (25), i.e., $\mathbf{H}_{\lambda\,\Delta L,\kappa\,\Delta K} = \sum_{m=0}^{D-1}\sum_{i=-J/2}^{J/2-1} \mathbf{G}_{m,i}\, u_{m,i}[\lambda,\kappa]$. The proposed basis optimization methodology extends the methodology presented for "simple" (i.e., single-channel and nonstructured) sparsity in [26] to the

present case of joint group sparsity. We note that separate extensions to group sparsity and to joint sparsity were presented in [33] and [34], respectively.

A. Basis Optimization Framework

Following [26], we set

$$u_{m,i}[\lambda,\kappa] \triangleq \frac{1}{\sqrt{D}}\, v_{m,i}[\lambda]\, e^{-j2\pi\frac{\kappa m}{D}}, \tag{55}$$

where $\{v_{m,i}[\lambda]\}_{i=-J/2}^{J/2-1}$ is an orthonormal 1D basis for each $m \in \{0,\ldots,D-1\}$. With respect to its dependence on κ, $\{u_{m,i}[\lambda,\kappa]\}$ conforms to the 2D Fourier basis underlying (24); however, the λ dependence is now defined by the 1D basis functions $v_{m,i}[\lambda]$ and generally different from that of the 2D Fourier basis. We use the Fourier basis with respect to κ because it already yields excellent joint group sparsity; this is due to the fact that the leakage effects in the m direction are relatively weak because of the rather rapid decay of the function $\phi^{(\nu)}(x)$ (as noted below (43)). Thus, little improvement of the joint group sparsity can be achieved by an explicit optimization of the κ dependence. However, using the Fourier basis with respect to λ would yield poor joint group sparsity; this is due to the fact that the leakage effects in the i direction are relatively strong because of the slow decay of the function $\psi(x)$ (again as noted below (43)). This motivates the use of optimized 1D basis functions $v_{m,i}[\lambda]$.

Our development is motivated by the channel model (41); however, we do not require knowledge of the channel parameters P, $\eta_p^{(\theta)}$, $\tau_p^{(\theta)}$, and $\nu_p^{(\theta)}$. More specifically, to set up the optimization framework, we consider elementary single-scatterer channels $h^{(\theta)}(t,\tau) = \delta(\tau-\tau_1^{(\theta)})\, e^{j2\pi\nu_1^{(\theta)}t}$, $\theta \in \Theta$. Since the parameters $\tau_1^{(\theta)}$ and $\nu_1^{(\theta)}$ are unknown, we model them as random variables that are distributed according to some known probability density function (pdf) $p(\boldsymbol{\tau}_1,\boldsymbol{\nu}_1) \triangleq p\big(\tau_1^{(\theta_1)},\ldots,\tau_1^{(\theta_{N_{\mathrm{T}}N_{\mathrm{R}}})},\nu_1^{(\theta_1)},\ldots,\nu_1^{(\theta_{N_{\mathrm{T}}N_{\mathrm{R}}})}\big)$. The resulting "statistical" basis design takes into account *a priori* knowledge about the distribution of the delays and Doppler frequency shifts. If such knowledge is unavailable, a "nonstatistical" design is easily obtained by formally using an "uninformative" pdf, e.g., a uniform distribution on some feasible default region of possible delays and Doppler frequency shifts. We emphasize that the optimized basis is not restricted to a specular channel model of the form (41) but can be used for general doubly selective MIMO channels as defined in (3).

We now discuss the optimization of the 1D basis functions $v_{m,i}[\lambda]$. Consider a given 2D tiling $\{\mathcal{B}_b\}_{b=1}^B$ with corresponding 1D partition $\mathcal{J} = \{\mathcal{I}_b\}_{b=1}^B$ of $\{1,\ldots,JD\}$ defined by the groups $\mathcal{I}_b = \mathsf{S}(\mathcal{B}_b)$ (see (54)). Our goal is to find $\{v_{m,i}[\lambda]\}_{i=-J/2}^{J/2-1}$, $m \in \{0,\ldots,D-1\}$ such that, for the *random* single-scatterer channels $h^{(\theta)}(t,\tau)$ discussed above, the vectors $\mathrm{rvec}_{m,i}\big\{G_{m,i}^{(\theta)}\big\}$, $\theta \in \Theta$ are maximally jointly group sparse with respect

to $\mathcal{J}$ *on average*. Let us denote by $\mathbf{G} \in \mathbb{C}^{JD\times N_{\mathrm{T}}N_{\mathrm{R}}}$ the matrix with columns $\mathrm{rvec}_{m,i}\{G_{m,i}^{(\theta)}\}$, i.e.,

$$[\mathbf{G}]_{\mathsf{S}(m,i),\xi} = G_{m,i}^{(\theta_\xi)}\,, \qquad \xi \in \{1,\ldots,|\Theta|\} = \{1,\ldots,N_{\mathrm{T}}N_{\mathrm{R}}\}\,. \tag{56}$$

Motivated by (M)GCS theory—see Sections III-A and III-C—we measure the joint group sparsity of $\mathrm{rvec}_{m,i}\{G_{m,i}^{(\theta)}\}$, $\theta\in\Theta$ with respect to $\mathcal{J}$ by

$$\|\mathbf{G}\|_{\mathrm{F}|\mathcal{J}} \triangleq \sum_{b=1}^{B}\sqrt{\sum_{(m,i)\in\mathcal{B}_b}\sum_{\theta\in\Theta}|G_{m,i}^{(\theta)}|^2}\,. \tag{57}$$

We note for later use that this norm can also be written as

$$\|\mathbf{G}\|_{\mathrm{F}|\mathcal{J}} = \sum_{b=1}^{B}\|\mathbf{G}[b]\|_{\mathrm{F}}\,, \tag{58}$$

where $\mathbf{G}[b] \in \mathbb{C}^{|\mathcal{I}_b|\times|\Theta|}$ denotes the matrix that is constituted by the rows of $\mathbf{G}$ indexed by $\mathcal{I}_b$ and $\|\cdot\|_{\mathrm{F}}$ denotes the Frobenius norm. Furthermore, $\|\mathbf{G}\|_{\mathrm{F}|\mathcal{J}} = \|\mathbf{g}\|_{2,\tilde{\mathcal{J}}}$, where $\mathbf{g} \triangleq \big(\mathbf{g}^{(\theta_1)T}\cdots\mathbf{g}^{(\theta_{|\Theta|})T}\big)^T$ with $\mathbf{g}^{(\theta)} \triangleq \mathrm{rvec}_{m,i}\{G_{m,i}^{(\theta)}\}$ corresponds to the stacking explained in Section III-A and the associated partition $\tilde{\mathcal{J}}$ of $\{1,\ldots,JDN_{\mathrm{T}}N_{\mathrm{R}}\}$ defined in Section III-C is used.

We aim to minimize $\mathbb{E}\{\|\mathbf{G}\|_{\mathrm{F}|\mathcal{J}}\}$ with respect to the family of orthonormal 1-D bases $\{v_{m,i}[\lambda]\}_{i=-J/2}^{J/2-1}$, $m\in\{0,\ldots,D{-}1\}$, where $\mathbb{E}$ denotes the expectation with respect to $(\boldsymbol{\tau}_1,\boldsymbol{\nu}_1)$. This problem can be reformulated as follows. Let $\mathbf{V} \triangleq \mathrm{diag}\{\mathbf{V}_0,\ldots,\mathbf{V}_{D-1}\} \in \mathbb{C}^{JD\times JD}$ be the unitary block diagonal matrix with blocks $\mathbf{V}_m \in \mathbb{C}^{J\times J}$ given by $[\mathbf{V}_m]_{i+J/2+1,\,\lambda+1} \triangleq v_{m,i}^*[\lambda]$, $i\in\{-J/2,\ldots,J/2-1\}$, $\lambda\in\{0,\ldots,J-1\}$, for $m\in\{0,\ldots,D{-}1\}$. Furthermore, let

$$C^{(\nu)}[m,\lambda] \triangleq \sum_{i=-J/2}^{J/2-1}\sum_{q=0}^{N-1}\psi^{(\nu)}(i+qL)\,A_{\gamma,g}^*\!\left(m,\frac{i+qL}{L_{\mathrm{r}}}\right)e^{j2\pi\frac{\lambda i}{J}}, \tag{59}$$

with $\psi^{(\nu)}(i) \triangleq e^{j\pi(\nu T_{\mathrm{s}}-\frac{i}{L_{\mathrm{r}}})(L_{\mathrm{r}}-1)}\psi(i-\nu T_{\mathrm{s}}L_{\mathrm{r}})$, and define the vectors

$$\mathbf{c}_m(\tau,\nu) \triangleq \sqrt{D}\,\phi^{(\nu)}\!\left(m-\frac{\tau}{T_{\mathrm{s}}}\right)\big(C^{(\nu)}[m,0]\cdots C^{(\nu)}[m,J{-}1]\big)^T$$

and, in turn, the vector $\mathbf{c}(\tau,\nu) \triangleq \big(\mathbf{c}_0^T(\tau,\nu)\cdots\mathbf{c}_{D-1}^T(\tau,\nu)\big)^T$. Finally, we evaluate $\mathbf{c}(\tau,\nu)$ at the delays $\tau_1^{(\theta)}$ and Doppler frequency shifts $\nu_1^{(\theta)}$ for all components θ of our single-scatterer MIMO channel and arrange the resulting vectors $\mathbf{c}\big(\tau_1^{(\theta_\xi)},\nu_1^{(\theta_\xi)}\big)$, $\xi\in\{1,\ldots,N_{\mathrm{T}}N_{\mathrm{R}}\}$ into the matrix

$$\mathbf{C}(\boldsymbol{\tau}_1,\boldsymbol{\nu}_1) \triangleq \Big(\mathbf{c}\big(\tau_1^{(\theta_1)},\nu_1^{(\theta_1)}\big)\;\mathbf{c}\big(\tau_1^{(\theta_2)},\nu_1^{(\theta_2)}\big)\cdots\mathbf{c}\big(\tau_1^{(\theta_{N_{\mathrm{T}}N_{\mathrm{R}}})},\nu_1^{(\theta_{N_{\mathrm{T}}N_{\mathrm{R}}})}\big)\Big) \in \mathbb{C}^{JD\times N_{\mathrm{T}}N_{\mathrm{R}}}\,.$$

Then, it is shown in Appendix C that

$$\mathbf{G} = \mathbf{V}\mathbf{C}(\boldsymbol{\tau}_1,\boldsymbol{\nu}_1)\,, \tag{60}$$

so that we can reformulate our minimization problem as

$$\hat{\mathbf{V}}_{\text{opt}} = \underset{\mathbf{V}\in\mathcal{U}^{\text{bl}}}{\arg\min}\, \mathbb{E}\big\{\|\mathbf{VC}(\boldsymbol{\tau}_1,\boldsymbol{\nu}_1)\|_{\text{F}|\mathcal{J}}\big\}\,. \tag{61}$$

Here, $\mathcal{U}^{\text{bl}}$ denotes the set of unitary block diagonal $JD\times JD$ matrices with blocks of equal size $J\times J$ on the diagonal. Finally, with a view towards a numerical algorithm, we use the following Monte-Carlo approximation of (61):

$$\hat{\mathbf{V}} = \underset{\mathbf{V}\in\mathcal{U}^{\text{bl}}}{\arg\min} \sum_{\rho} \|\mathbf{VC}((\boldsymbol{\tau}_1,\boldsymbol{\nu}_1)_\rho)\|_{\text{F}|\mathcal{J}}\,, \tag{62}$$

where the $(\boldsymbol{\tau}_1,\boldsymbol{\nu}_1)_\rho$ denote samples of the random vector $(\boldsymbol{\tau}_1,\boldsymbol{\nu}_1)$ independently drawn from its pdf $p(\boldsymbol{\tau}_1,\boldsymbol{\nu}_1)$.

B. Basis Optimization Algorithm

Because the set $\mathcal{U}^{\text{bl}}$ is not convex, the minimization problem (62) is not convex. An approximate solution can be obtained by an algorithm that extends the basis optimization algorithm presented for single-channel, nonstructured sparsity in [26] to the present case of joint group sparsity. We first exploit the fact that (62)—which is a minimization problem of dimension DJ^2—can be decomposed into $D/\Delta m'$ separate minimization problems of dimension $\Delta m' J^2$ each. To obtain this decomposition, we first partition the set $\{0,\ldots,D-1\}$ into the $D/\Delta m'$ pairwise disjoint subsets $\mathcal{M}_{b'} \triangleq \{(b'-1)\Delta m', (b'-1)\Delta m'+1,\ldots,b'\Delta m'-1\}$, for $b'\in\{1,\ldots,D/\Delta m'\}$, and we consider the $D/\Delta m'$ sets $\mathcal{A}_{b'}$, $b'\in\{1,\ldots,D/\Delta m'\}$ that consist of the indices b of all those $J/\Delta i'$ blocks $\mathcal{B}_b$ that contain pairs (m,i) with $m\in\mathcal{M}_{b'}$, i.e., $\mathcal{A}_{b'} \triangleq \big\{b\in\{1,\ldots,B\}\,\big|\,\exists\, m\in\mathcal{M}_{b'}$ such that $(m,i)\in\mathcal{B}_b\big\}$. (In Figure 2, $\mathcal{A}_{b'}$ corresponds to all the blocks placed on top of each other in the b'th vertical column within the fundamental domain.) Now recall (cf. (58)) that

$$\|\mathbf{VC}(\boldsymbol{\tau}_1,\boldsymbol{\nu}_1)\|_{\text{F}|\mathcal{J}} = \sum_{b=1}^{B} \big\|\big(\mathbf{VC}(\boldsymbol{\tau}_1,\boldsymbol{\nu}_1)\big)[b]\big\|_{\text{F}}\,, \tag{63}$$

where $\big(\mathbf{VC}(\boldsymbol{\tau}_1,\boldsymbol{\nu}_1)\big)[b]\in\mathbb{C}^{|\mathcal{I}_b|\times N_{\text{T}}N_{\text{R}}}$ denotes the matrix that is constituted by the rows of $\mathbf{VC}(\boldsymbol{\tau}_1,\boldsymbol{\nu}_1)$ indexed by $\mathcal{I}_b = \mathsf{S}(\mathcal{B}_b)$. Furthermore, note that due to the block-diagonal structure of $\mathbf{V}$, we have $\mathbf{VC}(\boldsymbol{\tau}_1,\boldsymbol{\nu}_1) = \big(\big(\mathbf{V}_0\mathbf{C}_0(\boldsymbol{\tau}_1,\boldsymbol{\nu}_1)\big)^T\cdots\big(\mathbf{V}_{D-1}\mathbf{C}_{D-1}(\boldsymbol{\tau}_1,\boldsymbol{\nu}_1)\big)^T\big)^T$ with $\mathbf{C}_m(\boldsymbol{\tau}_1,\boldsymbol{\nu}_1) \triangleq \Big(\mathbf{c}_m\big(\tau_1^{(\theta_1)},\nu_1^{(\theta_1)}\big)\;\cdots\;\mathbf{c}_m\big(\tau_1^{(\theta_{N_{\text{T}}N_{\text{R}}})},\nu_1^{(\theta_{N_{\text{T}}N_{\text{R}}})}\big)\Big)$. It follows that each summand $\big\|\big(\mathbf{VC}(\boldsymbol{\tau}_1,\boldsymbol{\nu}_1)\big)[b]\big\|_{\text{F}}$ in (63) involves only the submatrices $\mathbf{V}_m\mathbf{C}_m(\boldsymbol{\tau}_1,\boldsymbol{\nu}_1)$ of $\mathbf{VC}(\boldsymbol{\tau}_1,\boldsymbol{\nu}_1)$ for those m for which there is an $i\in\{-J/2,\ldots,J/2-1\}$ such that $\mathsf{S}(m,i)\in\mathcal{I}_b$ (or equivalently $(m,i)\in\mathcal{B}_b$). Therefore, for any fixed $b'\in\{1,\ldots,D/\Delta m'\}$, the set of summands $\big\{\big\|\big(\mathbf{VC}(\boldsymbol{\tau}_1,\boldsymbol{\nu}_1)\big)[b]\big\|_{\text{F}}\big\}_{b\in\mathcal{A}_{b'}}$ involves exactly the set of submatrices $\big\{\mathbf{V}_m\mathbf{C}_m(\boldsymbol{\tau}_1,\boldsymbol{\nu}_1)\big\}_{m\in\mathcal{M}_{b'}}$. As a consequence, a reordering of the

summands in (63) yields

$$\sum_{b=1}^{B} \big\| \big(\mathbf{VC}(\boldsymbol{\tau}_1, \boldsymbol{\nu}_1)\big)[b] \big\|_{\mathrm{F}} = \sum_{b'=1}^{D/\Delta m'} \sum_{b \in \mathcal{A}_{b'}} \big\| \big(\mathbf{VC}(\boldsymbol{\tau}_1, \boldsymbol{\nu}_1)\big)[b] \big\|_{\mathrm{F}} . \tag{64}$$

Finally, using (63) and (64), the function minimized in (62) can be developed as

$$\sum_{\rho} \|\mathbf{VC}((\boldsymbol{\tau}_1, \boldsymbol{\nu}_1)_\rho)\|_{\mathrm{F}|\mathcal{J}} = \sum_{\rho} \sum_{b'=1}^{D/\Delta m'} \sum_{b \in \mathcal{A}_{b'}} \big\| \big(\mathbf{VC}((\boldsymbol{\tau}_1, \boldsymbol{\nu}_1)_\rho)\big)[b] \big\|_{\mathrm{F}} = \sum_{b'=1}^{D/\Delta m'} Y_{b'}\big(\{\mathbf{V}_m\}_{m \in \mathcal{M}_{b'}}\big) ,$$

with

$$\begin{aligned} Y_{b'}\big(\{\mathbf{V}_m\}_{m \in \mathcal{M}_{b'}}\big) &\triangleq \sum_{\rho} \sum_{b \in \mathcal{A}_{b'}} \big\| \big(\mathbf{VC}((\boldsymbol{\tau}_1, \boldsymbol{\nu}_1)_\rho)\big)[b] \big\|_{\mathrm{F}} \\ &= \sum_{\rho} \sum_{b \in \mathcal{A}_{b'}} \sqrt{\sum_{\xi=1}^{N_{\mathrm{T}} N_{\mathrm{R}}} \sum_{(m,i) \in \mathcal{B}_b} \big| \big[\mathbf{VC}((\boldsymbol{\tau}_1, \boldsymbol{\nu}_1)_\rho)\big]_{\mathsf{S}(m,i),\xi} \big|^2} \\ &= \sum_{\rho} \sum_{b \in \mathcal{A}_{b'}} \sqrt{\sum_{\xi=1}^{N_{\mathrm{T}} N_{\mathrm{R}}} \sum_{m \in \mathcal{M}_{b'}} \sum_{i:(m,i) \in \mathcal{B}_b} \big| \big[\mathbf{V}_m \mathbf{C}_m((\boldsymbol{\tau}_1, \boldsymbol{\nu}_1)_\rho)\big]_{i+J/2+1,\xi} \big|^2} . \end{aligned}$$

Because $Y_{b'}\big(\{\mathbf{V}_m\}_{m \in \mathcal{M}_{b'}}\big)$ involves only the matrices $\mathbf{V}_m$ for $m \in \mathcal{M}_{b'}$ and the sets $\mathcal{M}_{b'}$ are pairwise disjoint, the minimization problem (62) reduces to the $D/\Delta m'$ separate minimization problems

$$\{\hat{\mathbf{V}}_m\}_{m \in \mathcal{M}_{b'}} = \arg\min\, Y_{b'}\big(\{\mathbf{V}_m\}_{m \in \mathcal{M}_{b'}}\big) , \qquad b' \in \{1, \ldots, D/\Delta m'\} . \tag{65}$$

Here, the minimization is with respect to $\{\mathbf{V}_m\}_{m \in \mathcal{M}_{b'}}$ with $\mathbf{V}_m \in \mathcal{U}$, where $\mathcal{U}$ denotes the *nonconvex* set of unitary $J \times J$ matrices. Note that each minimization problem in (65) is only of dimension $\Delta m' J^2$, since $|\mathcal{M}_{b'}| = \Delta m'$ and $\mathbf{V}_m \in \mathbb{C}^{J \times J}$, whereas the minimization problem (62) has dimension DJ^2. Typically, $\Delta m'$ is quite small because of the fast decay of $\phi^{(\nu^{(\theta)})}(m - \tau^{(\theta)}/T_{\mathrm{s}})$. The final matrix $\hat{\mathbf{V}} \in \mathbb{C}^{JD \times JD}$ minimizing (62) is then given as $\hat{\mathbf{V}} = \mathrm{diag}\{\hat{\mathbf{V}}_0, \ldots, \hat{\mathbf{V}}_{D-1}\}$.

In order to (approximately) solve (65), we build on the fact that every unitary matrix $\mathbf{V}_m \in \mathcal{U}$ can be represented as $\mathbf{V}_m = e^{j\mathbf{A}_m}$, where $\mathbf{A}_m$ is a Hermitian $J \times J$ matrix, and the matrix exponential $e^{j\mathbf{A}_m}$ can be approximated by its first-order Taylor series expansion [73]. Thus, we obtain $\mathbf{V}_m \approx \mathbf{I}_J + j\mathbf{A}_m$, where $\mathbf{I}_J$ denotes the $J \times J$ identity matrix. This approximation will be good only if $\mathbf{A}_m$ is sufficiently "small." Therefore, following [26], for each (fixed) $b' \in \{1, \ldots, D/\Delta m'\}$, we construct $\{\mathbf{V}_m\}_{m \in \mathcal{M}_{b'}}$ iteratively by performing a sequence of *small* updates, using the approximations $\mathbf{V}_m \approx \mathbf{I}_J + j\mathbf{A}_m$ in the optimization criterion but not for actually updating $\mathbf{V}_m$, in order to guarantee that the iterated $\mathbf{V}_m$ are always unitary. The resulting iterative basis optimization algorithm is a straightforward adaptation of the algorithm presented in [26] and will be stated without further discussion. In what follows, we consider a fixed $b' \in \{1, \ldots, D/\Delta m'\}$.

- ***Input*:** Initialization matrices $\{\mathbf{V}_m^{\text{init}}\}_{m\in\mathcal{M}_{b'}}$, minimization function $Y_{b'}(\cdot)$, threshold ε
- ***Initialization*:** $n=0$, $\mathbf{V}_m^{(0)}=\mathbf{V}_m^{\text{init}}$, $\varepsilon^{(0)}=\varepsilon$
- ***Iteration*:** **while** stopping criterion is not met **do**

  1) Solve the *convex* problem

$$\left\{\hat{\mathbf{A}}_m^{(n)}\right\}_{m\in\mathcal{M}_{b'}} = \underset{\{\mathbf{A}_m^{(n)}\}_{m\in\mathcal{M}_{b'}}\in\mathcal{A}^{(n)}}{\arg\min} Y_{b'}\left(\left\{(\mathbf{I}_J+j\mathbf{A}_m)\mathbf{V}_m^{(n)}\right\}_{m\in\mathcal{M}_{b'}}\right), \tag{66}$$

  where $\mathcal{A}^{(n)}$ denotes the set of all sets of $|\mathcal{M}_{b'}|=\Delta m'$ Hermitian $J\times J$ matrices $\mathbf{A}$ satisfying $\max_{i,j}|[\mathbf{A}]_{i,j}|<\varepsilon^{(n)}$

  2) **if** $Y_{b'}\left(\left\{e^{j\hat{\mathbf{A}}_m^{(n)}}\mathbf{V}_m^{(n)}\right\}_{m\in\mathcal{M}_{b'}}\right) < Y_{b'}\left(\left\{\mathbf{V}_m^{(n)}\right\}_{m\in\mathcal{M}_{b'}}\right)$, set $\mathbf{V}_m^{(n+1)}=e^{j\hat{\mathbf{A}}_m^{(n)}}\mathbf{V}_m^{(n)}$, $m\in\mathcal{M}_{b'}$ and $\varepsilon^{(n+1)}=\varepsilon^{(n)}$

  else set $\mathbf{V}_m^{(n+1)}=\mathbf{V}_m^{(n)}$, $m\in\mathcal{M}_{b'}$ and $\varepsilon^{(n+1)}=\varepsilon^{(n)}/2$

  3) $n\mapsto n+1$

- ***Output*:** $\left\{\mathbf{V}_m^{(n)}\right\}_{m\in\mathcal{M}_{b'}}$

The algorithm is stopped either if the threshold $\varepsilon^{(n)}$ falls below a prescribed value or if a prescribed maximum number of iterations has been performed. The initialization matrices $\mathbf{V}_m^{\text{init}}$ are chosen as unitary $J\times J$ DFT matrices. For this choice, the analysis in Section V shows that the coefficients $G_{m,i}^{(\theta)}=\sqrt{JD}\,F_{m,i}^{(\theta)}$ are already jointly group sparse to a certain degree. The convex problem (66) can be solved by standard convex optimization techniques [74].

Finally, we note that the basis optimization does not involve the receive signal, and thus it has to be performed only once before the start of data transmission.

VII. Simulation Results

We present simulation results demonstrating the performance gains of the proposed MGCS channel estimator relative to the conventional compressive channel estimator described in [26].

A. Simulation Setup

We simulated CP OFDM and CP MIMO-OFDM systems with $K=512$ subcarriers, symbol duration $N=640$, CP length $N-K=128$, carrier frequency $f_0=5\,\text{GHz}$, transmit bandwidth $1/T_{\text{s}}=5\,\text{MHz}$, and $L=32$ transmitted OFDM symbols. The number of transmit and receive antennas was $N_{\text{T}}=N_{\text{R}}\in\{1,2,3,4\}$.

The interpolation/anti-aliasing filters $f_1(t) = f_2(t)$ were chosen as root-raised-cosine filters with roll-off factor 0.25. The size of the pilot sets was $Q = |\mathcal{P}^{(s)}| = 1024$ ($s \in \{1, \ldots, N_\mathrm{T}\}$). Thus, the total number of pilot symbols was $QN_\mathrm{T}^2 = 1024 \cdot N_\mathrm{T}^2$, corresponding to a fraction of $6.25 \cdot N_\mathrm{T}\,\%$ of all the $KLN_\mathrm{T} = 16.384 \cdot N_\mathrm{T}$ transmitted symbols. The pilot time-frequency positions $\mu_q^{(s)}$ ($q \in \{1, \ldots, Q\}$, $s \in \{1, \ldots, N_\mathrm{T}\}$) were chosen uniformly at random from a subsampled time-frequency grid $\mathcal{G}$ with spacings $\Delta L = 1$ and $\Delta K = 4$, and partitioned into N_T pairwise disjoint pilot time-frequency position sets $\mathcal{P}^{(s)}$ ($s \in \{1, \ldots, N_\mathrm{T}\}$) of size $Q = 1024$ each. The pilot matrix $\mathbf{P} = \big(\mathbf{p}^{(1)} \cdots \mathbf{p}^{(N_\mathrm{T})}\big)$ had a constant diagonal and was zero otherwise; the pilot (QPSK) symbol on the diagonal was scaled such that its power was equal to the total power of N_T data (QPSK) symbols.

We used the geometry-based channel simulation tool IlmProp [75] to generate 500 realizations of a doubly selective SISO or MIMO channel during blocks of $L = 32$ OFDM symbols. Transmitter and receiver were separated by about 1500 m. Seven clusters of ten specular scatterers each were randomly placed in an area of size 2500 m $\times$ 800 m; additionally, three clusters of ten specular scatterers each were randomly placed within a circle of radius 100 m around the receiver. For each cluster and for the receiver, the speed was uniformly distributed between 0 and 50 m/s, the acceleration was uniformly distributed between 0 and 7 m/s^2, and the directions (angles) of the velocity and acceleration vectors were uniformly distributed between 0° and 360°. In the MIMO case, the transmit antennas as well as the receive antennas were spaced $c/(2f_0)$ apart. The noise $\mathbf{z}[n]$ in (6) was white with respect to n, independent across the vector entries, and circularly symmetric complex Gaussian with component variance σ_z chosen such that a prescribed receive signal-to-noise-ratio (SNR) was achieved. Here, the SNR is defined as the mean received signal power averaged over one block of length LN and all receive antennas, divided by σ_z^2.

The reconstruction method employed by the proposed channel estimator was G-BPDN or G-OMP in the SISO case and G-BPDN (operating in MGCS mode, cf. Section III-C), DCS-SOMP, or G-DCS-SOMP in the MIMO case. The results of G-CoSaMP are not shown for the sake of clarity of the figures; the performance of G-CoSaMP was observed to be intermediate between that of G-BPDN and that of G-DCS-SOMP. We used both the 2D DFT basis and optimized bases $\{u_{m,i}[\lambda, \kappa]\}$ that were calculated as described in Section VI. The pdf underlying this calculation was constructed as $p(\boldsymbol{\tau}_1, \boldsymbol{\nu}_1) = p\big(\tau_1^{(\theta_1)}, \nu_1^{(\theta_1)}\big)\, p\big(\tau_1^{(\theta_2)}, \nu_1^{(\theta_2)} \big| \tau_1^{(\theta_1)}, \nu_1^{(\theta_1)}\big) \cdots p\big(\tau_1^{(\theta_{N_\mathrm{T}N_\mathrm{R}})}, \nu_1^{(\theta_{N_\mathrm{T}N_\mathrm{R}})} \big| \tau_1^{(\theta_1)}, \nu_1^{(\theta_1)}\big)$, where each factor was uniform in a rectangular region. The region for the first factor was $[0, \tau_{\max}] \times [-\nu_{\max}, \nu_{\max}]$, where $\tau_{\max} = 25.6\mu s$ is the length of the cyclic prefix and $\nu_{\max} \approx 293$ Hz was determined as 3% of the subcarrier spacing. The regions for the remaining factors were $\{0\} \times [-1.4, 1.4]$ Hz, i.e., the time delays of the individual component channels were supposed equal whereas the Doppler frequency

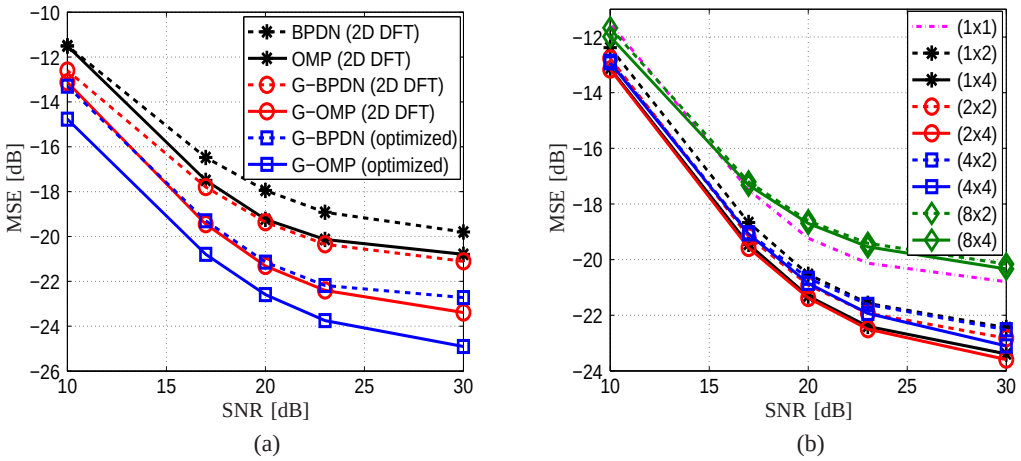

Fig. 4. MSE versus SNR for various compressive estimators in the SISO case: (a) using different CS reconstruction methods, the 2D DFT basis and the optimized basis, and block size $\Delta m' \times \Delta i' = 1 \times 4$; (b) using G-OMP, the 2D DFT basis, and different block sizes $\Delta m' \times \Delta i'$.

shifts were allowed to differ by at most ± 1.4 Hz.

The channel estimation performance was measured by the empirical mean square error (MSE) normalized by the mean energy of the channel coefficients.

B. Performance Gains Achieved by Leveraging Group Sparsity

For the SISO case, we compare the performance of the proposed compressive channel estimator leveraging group sparsity—i.e., using G-BPDN or G-OMP as GCS reconstruction method—with that of the conventional compressive channel estimator using BPDN or OMP [26]. Figure 4(a) shows the channel estimation MSE versus the SNR. The blocks $\mathcal{B}_b$ of the delay-Doppler tiling used in the definition of group sparsity (see Section V-A) were of size $\Delta m' \times \Delta i' = 1 \times 4$. For the proposed channel estimator, we used both the 2D DFT basis and the optimized basis. It is seen that exploiting the inherent group sparsity of the channel yields a substantial reduction of the MSE, and an additional substantial MSE reduction is obtained by using the optimized basis.

Figure 4(b) shows the MSE versus the SNR for the proposed channel estimator using G-OMP, the 2D DFT basis, and different block sizes $\Delta m' \times \Delta i'$ (note that the case $\Delta m' \times \Delta i' = 1 \times 1$ corresponds to the conventional compressive channel estimator of [26]). One can observe a strong dependence of the performance on the block size. This can be explained by the fact that if the blocks $\mathcal{B}_b$ are chosen too large in a certain direction, many entries not belonging to the (effective) support of $\tilde{\mathbf{x}}$ in (39) will be assigned nonzero values during reconstruction since they belong to blocks containing some large entries.

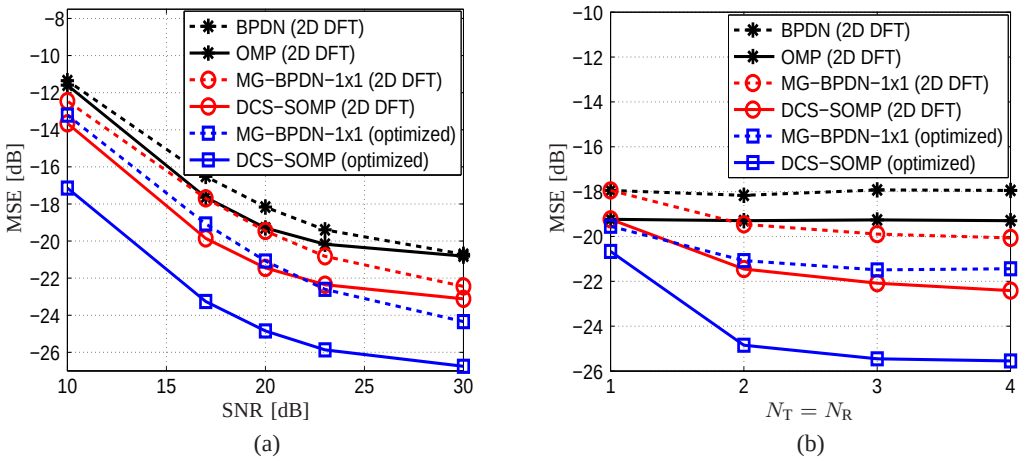

Fig. 5. MSE performance of various compressive estimators in the MIMO case: (a) MSE versus SNR for a 2×2 MIMO system, (b) MSE versus the number $N_T = N_R$ of transmit/receive antennas at an SNR of 20 dB.

C. Performance Gains Achieved by Leveraging Joint Sparsity

Next, we consider the MIMO case. We compare the proposed MCS channel estimator leveraging joint sparsity with the conventional compressive channel estimator. At this point, the proposed estimator does not exploit group sparsity; it uses G-BPDN or DCS-SOMP, where G-BPDN is based on blocks $\mathcal{B}_b$ of size $\Delta m' \times \Delta i' = 1\times1$ but runs in MGCS mode in order to exploit joint sparsity (this will be abbreviated as "MG-BPDN-1×1"). The reason for choosing MG-BPDN-1×1 instead of M-BPDN is its ability to handle the different measurement matrices $\mathbf{\Phi}^{(\theta)}$ in (18) (note that our application involves different measurement matrices, cf. (30)). The conventional compressive channel estimator uses BPDN or OMP for each component channel individually.

Figure 5(a) shows the channel estimation MSE versus the SNR for a MIMO system with $N_T = N_R = 2$ transmit and receive antennas. It is seen that substantial reductions of the MSE are obtained by taking advantage of the joint sparsity of the channel via MCS methods and, additionally, by using the optimized basis. Figure 5(b) shows the MSE versus the number $N_T = N_R \in \{1, 2, 3, 4\}$ of transmit/receive antennas at a fixed SNR of 20 dB. It is here seen that the performance of the proposed multichannel estimators improves when the number of transmit/receive antennas increases. This is because the estimation of the joint support becomes more accurate when a larger number of jointly sparse signals are available; this behavior has been studied in [76] for M-BPDN and SOMP. The flattening of the MSE curves is caused by the fact that the component channels, besides being jointly sparse in the sense of similar effective supports, are also similar with respect to the values of their nonzero entries. As explained in [76], the case where all jointly sparse signals are equal is a worst-case scenario for MCS, since no additional support information can be gained from additional signals. In our case, this effect is alleviated because the jointly sparse signals are observed through N_T different measurement matrices $\mathbf{\Phi}^{(s)}$,

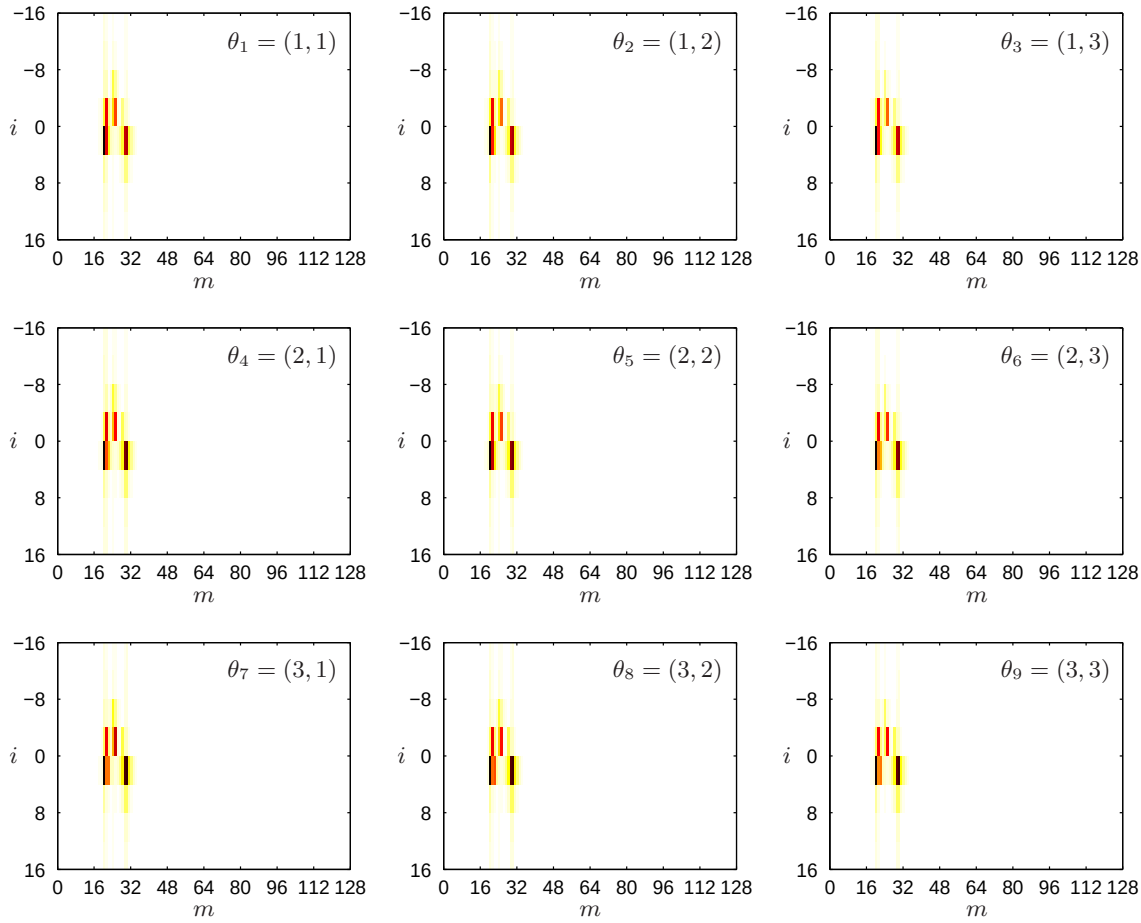

Fig. 6. Visualization of the joint group sparsity of the 2D DFT coefficients $F_{m,i}^{(\theta)}$ for a 3×3 MIMO system and block size $\Delta m' \times \Delta i' = 1 \times 4$.

$s \in \{1, \ldots, N_{\mathrm{T}}\}$. The performance of the conventional compressive channel estimator is essentially independent of the number of antennas; the slight variations of the MSE observed in Figure 5(b) are due to the use of different pilot constellations for different numbers of antennas.

D. Performance Gains Achieved by Leveraging Joint Group Sparsity

Finally, we study the performance of the proposed MGCS channel estimator that fully leverages the available structure, i.e., the joint group sparsity of the expansion coefficients $F_{m,i}^{(\theta)}$ or $G_{m,i}^{(\theta)}$. Figure 6 shows the energy of the 2D DFT coefficients $F_{m,i}^{(\theta)}$ accumulated within blocks $\mathcal{B}_b$ of size $\Delta m' \times \Delta i' = 1 \times 4$ for the nine component channels $\theta = (1,1), (1,2), \ldots, (3,3)$ of a 3×3 MIMO system. It is seen that the $F_{m,i}^{(\theta)}$ are effectively supported on the same blocks for all component channels θ. This demonstrates the strong available joint group sparsity, and suggests that exploiting this structure through MGCS channel estimation can yield significant performance gains relative to conventional compressive channel estimation.

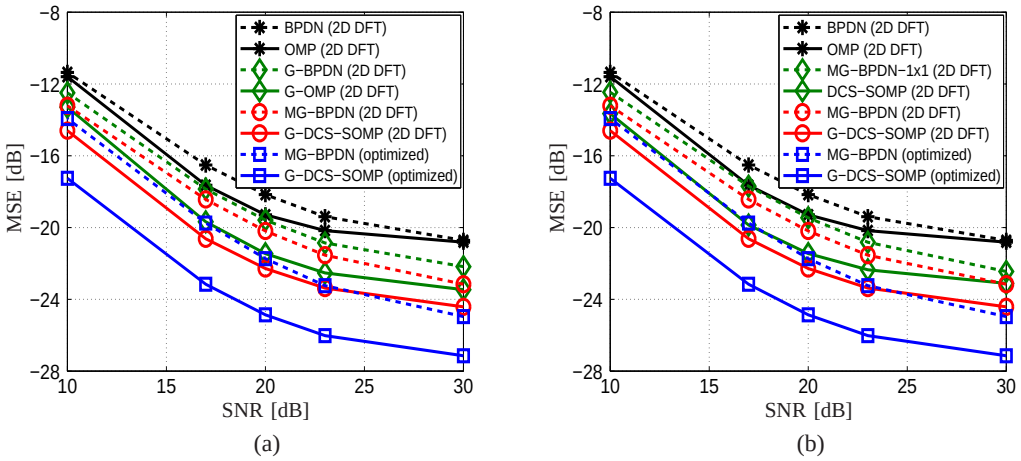

Fig. 7. MSE versus SNR for various compressive estimators and a 2×2 MIMO system: (a) MGCS estimator, GCS estimator, and conventional compressive estimator; (b) MGCS estimator, MCS estimator, and conventional compressive estimator.

To assess the actual performance gains, we simulated the MGCS estimator, the GCS estimator (leveraging only group sparsity), the MCS estimator (leveraging only joint sparsity), and the conventional compressive estimator for a 2×2 MIMO system. We used the 2D DFT basis for all estimators and additionally an optimized basis for the MGCS estimator. Figure 7 depicts the channel estimation MSE versus the SNR. Both parts (a) and (b) show identical MSE curves for the same versions of the MGCS estimator (using MG-BPDN or G-DCS-SOMP) and of the conventional compressive estimator (using BPDN or OMP); however, part (a) compares these curves with those obtained for the GCS estimator (using G-BPDN or G-OMP) whereas part (b) compares them with those obtained for the MCS estimator (using MG-BPDN-1×1 or DCS-SOMP). For the MGCS and GCS estimators, the blocks $\mathcal{B}_b$ were of size $\Delta m' \times \Delta i' = 1\times 4$. It can be seen that exploiting group sparsity or joint sparsity separately already outperforms conventional compressive channel estimation. Moreover, substantial additional performance gains are obtained by exploiting the joint group sparsity structure through the proposed MGCS estimator, and even larger gains are achieved when the MGCS estimator is used with an optimized basis.

VIII. Conclusion

Recent extensions of the basic methodology of compressed sensing (CS), such as group sparse CS (GCS) and multichannel CS (MCS), enable the development of advanced methods for compressive channel estimation. In this paper, we considered pulse-shaping multicarrier MIMO systems—which include MIMO-OFDM systems as a special case—transmitting over doubly selective MIMO channels. Extending our analysis in [26], we demonstrated that leakage effects induce an approximate *group* sparsity structure of the individual component channels in the delay-Doppler domain. We furthermore showed that the effective delay-Doppler supports of the

component channels overlap significantly, which implies that these channels can be considered approximately *jointly* group sparse. Motivated by this joint group sparsity structure, we developed the methodology of multichannel group sparse CS (MGCS) by combining GCS and MCS, and we devised an MGCS-based compressive channel estimator that leverages the joint group sparsity structure for improved performance. We also derived an upper bound on the MSE of the proposed MGCS-based channel estimator, and we analyzed the estimator's computational complexity.

For an additional improvement in performance, we proposed to replace the "default" Fourier basis used in the basic MGCS-based channel estimator by an alternative basis yielding reduced leakage effects and enhanced joint group sparsity. We presented an iterative algorithm for constructing such a basis using a criterion of maximum joint group sparsity and an approximation resulting in a sequence of convex programming problems. Statistical information about the channel can be incorporated in this algorithm if available. The basis is precomputed before the start of data transmission.

Simulations using a geometry-based channel simulator demonstrated significant performance gains relative to conventional compressive channel estimation. More specifically, we observed that large gains can be already obtained by leveraging only group sparsity or joint sparsity, and the combined MGCS approach yields a further substantial performance gain. An additional improvement in performance can be obtained by using the bases provided by the proposed basis optimization algorithm.

Interesting directions for further research include optimum choices of the parameters of CS reconstruction techniques (e.g., the parameter ϵ in G-BPDN or the number of iterations in G-OMP), improved pilot designs (i.e., choices of the positions and values of the pilots, cf. [77, 78]), and an extension of the compressive channel tracking method proposed in [79] to the joint group sparsity structure.

Acknowledgment

The authors would like to thank Professor Holger Rauhut for helpful comments.

Appendix A: Proof of Theorem 1

Let $\mathbf{h}^{(\theta)} \triangleq \operatorname{rvec}_{l,k}\{H_{l,k}^{(\theta)}\} \in \mathbb{C}^{KL}$, i.e., $[\mathbf{h}^{(\theta)}]_{k+lK+1} = H_{l,k}^{(\theta)}$; let $\mathbf{f}^{(\theta)} \triangleq \operatorname{rvec}_{m,i}\{F_{m,i}^{(\theta)}\} \in \mathbb{C}^{KL}$, i.e., $[\mathbf{f}^{(\theta)}]_{mL+i+L/2+1} = F_{m,i}^{(\theta)}$; and let $\mathbf{U}_{\mathrm{F}} \in \mathbb{C}^{KL\times KL}$ be the unitary matrix with entries $[\mathbf{U}_{\mathrm{F}}]_{k+lK+1,mL+i+L/2+1} = \frac{1}{\sqrt{KL}}\, e^{-j2\pi(\frac{km}{K}-\frac{li}{L})}$, where $l \in \{0,\dots,L-1\}$, $k \in \{0,\dots,K-1\}$, $m \in \{0,\dots,K-1\}$, and $i \in \{-L/2,\dots, L/2-1\}$. Then, (10) can be written as $\mathbf{h}^{(\theta)} = \sqrt{KL}\,\mathbf{U}_{\mathrm{F}}\,\mathbf{f}^{(\theta)}$, which implies

$$\|\mathbf{h}^{(\theta)}\|_2 = \sqrt{KL}\,\|\mathbf{f}^{(\theta)}\|_2\,. \tag{67}$$

Next, let $\mathbf{h}_{\Delta}^{(\theta)} \triangleq \mathrm{rvec}_{\lambda,\kappa}\{H_{\lambda\Delta L,\kappa\Delta K}^{(\theta)}\} \in \mathbb{C}^{JD}$, i.e., $[\mathbf{h}_{\Delta}^{(\theta)}]_{\kappa+\lambda D+1} = H_{\lambda\Delta L,\kappa\Delta K}^{(\theta)}$; let $\tilde{\mathbf{f}}^{(\theta)} \in \mathbb{C}^{JD}$ be defined by $[\tilde{\mathbf{f}}^{(\theta)}]_{mJ+i+J/2+1} = F_{m,i}^{(\theta)}$ (this is the subvector of $\mathbf{f}^{(\theta)}$ that corresponds to the restriction of $F_{m,i}^{(\theta)}$ to $\{0,\dots,D-1\} \times \{-J/2,\dots,J/2-1\}$); and let $\tilde{\mathbf{U}}_{\mathrm{F}} \in \mathbb{C}^{JD\times JD}$ be the unitary matrix with entries $[\tilde{\mathbf{U}}_{\mathrm{F}}]_{\kappa+\lambda D+1,mJ+i+J/2+1} = \frac{1}{\sqrt{JD}}\, e^{-j2\pi(\frac{\kappa m}{D}-\frac{\lambda i}{J})}$, where $\lambda \in \{0,\dots,J-1\}$, $\kappa \in \{0,\dots,D-1\}$, $m \in \{0,\dots,D-1\}$, and $i \in \{-J/2,\dots,J/2-1\}$. Then, we can rewrite (24) as $\mathbf{h}_{\Delta}^{(\theta)} = \sqrt{JD}\,\tilde{\mathbf{U}}_{\mathrm{F}}\tilde{\mathbf{f}}^{(\theta)}$. We thus obtain

$$\|\mathbf{h}_{\Delta}^{(\theta)}\|_2 = \sqrt{JD}\,\|\tilde{\mathbf{f}}^{(\theta)}\|_2 = \sqrt{JD}\,\|\mathbf{f}^{(\theta)}\|_2\,, \tag{68}$$

since $\mathbf{f}^{(\theta)}$ differs from its subvector $\tilde{\mathbf{f}}^{(\theta)}$ only by additional zero entries. Finally, let $\mathbf{g}^{(\theta)} \triangleq \mathrm{rvec}_{m,i}\{G_{m,i}^{(\theta)}\} \in \mathbb{C}^{JD}$, i.e., $[\mathbf{g}^{(\theta)}]_{mJ+i+J/2+1} = G_{m,i}^{(\theta)}$, and let $\mathbf{U} \in \mathbb{C}^{JD\times JD}$ be the unitary matrix with entries $[\mathbf{U}]_{\kappa+\lambda D+1,mJ+i+J/2+1} = u_{m,i}[\lambda,\kappa]$. Then (25) can be written as $\mathbf{h}_{\Delta}^{(\theta)} = \mathbf{U}\mathbf{g}^{(\theta)}$, which implies

$$\|\mathbf{h}_{\Delta}^{(\theta)}\|_2 = \|\mathbf{g}^{(\theta)}\|_2\,. \tag{69}$$

Combining (67)–(69), we obtain $\|\mathbf{h}^{(\theta)}\|_2 = \sqrt{\frac{KL}{JD}}\,\|\mathbf{g}^{(\theta)}\|_2$ and, furthermore,

$$\sqrt{\sum_{l=0}^{L-1}\sum_{k=0}^{K-1}|\hat{H}_{l,k}^{(\theta)} - H_{l,k}^{(\theta)}|^2} = \big\|\hat{\mathbf{h}}^{(\theta)} - \mathbf{h}^{(\theta)}\big\|_2 = \sqrt{\frac{KL}{JD}}\,\big\|\hat{\mathbf{g}}^{(\theta)} - \mathbf{g}^{(\theta)}\big\|_2\,, \tag{70}$$

where $\hat{\mathbf{h}}^{(\theta)} \triangleq \mathrm{rvec}_{l,k}\{\hat{H}_{l,k}^{(\theta)}\}$ and $\hat{\mathbf{g}}^{(\theta)} \triangleq \mathrm{rvec}_{m,i}\{\hat{G}_{m,i}^{(\theta)}\}$ denote the estimates of $\mathbf{h}^{(\theta)}$ and $\mathbf{g}^{(\theta)}$, respectively.

Next, let $\tilde{\mathbf{G}}_{m,i}$ be the $N_{\mathrm{R}} \times N_{\mathrm{T}}$ matrix with entries $\big[\tilde{\mathbf{G}}_{m,i}\big]_{r,s} \triangleq \tilde{G}_{m,i}^{(r,s)}$ for $r \in \{1,\dots,N_{\mathrm{R}}\}$ and $s \in \{1,\dots,N_{\mathrm{T}}\}$, and let (cf. (29))

$$\tilde{\mathbf{g}}^{(\theta)} \triangleq \mathrm{rvec}_{m,i}\{\tilde{G}_{m,i}^{(\theta)}\} = \sqrt{\frac{JD}{Q}}\,\mathbf{x}^{(\theta)}. \tag{71}$$

By the definition of $\tilde{G}_{m,i}^{(\theta)}$ in (26), we have $\tilde{\mathbf{G}}_{m,i} = \mathbf{G}_{m,i}\mathbf{P}$ and, in turn, $\mathbf{G}_{m,i} = \tilde{\mathbf{G}}_{m,i}\mathbf{P}^{-1}$. Similarly, we have $\hat{\mathbf{G}}_{m,i} = \hat{\tilde{\mathbf{G}}}_{m,i}\mathbf{P}^{-1}$, where $\hat{\tilde{\mathbf{G}}}_{m,i}$ denotes the estimate of $\tilde{\mathbf{G}}_{m,i}$ (cf. step 2 in Section IV-B). We then obtain

$$\begin{aligned}
\sum_{\theta\in\Theta}\big\|\hat{\mathbf{g}}^{(\theta)} - \mathbf{g}^{(\theta)}\big\|_2^2 &\overset{(a)}{=} \sum_{m=0}^{D-1}\sum_{i=-J/2}^{J/2-1}\big\|\hat{\mathbf{G}}_{m,i} - \mathbf{G}_{m,i}\big\|_{\mathrm{F}}^2 \\
&= \sum_{m=0}^{D-1}\sum_{i=-J/2}^{J/2-1}\big\|\big(\hat{\tilde{\mathbf{G}}}_{m,i} - \tilde{\mathbf{G}}_{m,i}\big)\mathbf{P}^{-1}\big\|_{\mathrm{F}}^2 \\
&\overset{(b)}{\le} \sum_{m=0}^{D-1}\sum_{i=-J/2}^{J/2-1}\big\|\hat{\tilde{\mathbf{G}}}_{m,i} - \tilde{\mathbf{G}}_{m,i}\big\|_{\mathrm{F}}^2\,\|\mathbf{P}^{-1}\|^2 \\
&\overset{(c)}{=} \|\mathbf{P}^{-1}\|^2\sum_{\theta\in\Theta}\big\|\hat{\tilde{\mathbf{g}}}^{(\theta)} - \tilde{\mathbf{g}}^{(\theta)}\big\|_2^2
\end{aligned}$$

$$= \|\mathbf{P}^{-1}\|^2 \frac{JD}{Q} \sum_{\theta\in\Theta} \left\|\hat{\mathbf{x}}^{(\theta)} - \mathbf{x}^{(\theta)}\right\|_2^2$$
$$= \frac{JD}{Q} \|\mathbf{P}^{-1}\|^2 \|\hat{\mathbf{x}} - \mathbf{x}\|_2^2 , \tag{72}$$

where $\|\cdot\|$ denotes the operator norm, $\mathbf{x} \triangleq \left(\mathbf{x}^{(\theta_1)T} \cdots \mathbf{x}^{(\theta_{N_\mathrm{T}N_\mathrm{R}})T}\right)^T$, and $\hat{\mathbf{x}} \triangleq \left(\hat{\mathbf{x}}^{(\theta_1)T} \cdots \hat{\mathbf{x}}^{(\theta_{N_\mathrm{T}N_\mathrm{R}})T}\right)^T$. Here, (a) and (c) are obtained by reordering the sums, and (b) follows by the general inequality $\|\mathbf{AB}\|_\mathrm{F} \leq \|\mathbf{A}\|_\mathrm{F}\|\mathbf{B}\|$ [67, problem 20 in ch. 5.6]. A combination of (70) and (72) then yields

$$E = \sqrt{\sum_{\theta\in\Theta} \sum_{l=0}^{L-1} \sum_{k=0}^{K-1} \left|\hat{H}_{l,k}^{(\theta)} - H_{l,k}^{(\theta)}\right|^2} = \sqrt{\sum_{\theta\in\Theta} \frac{KL}{JD} \left\|\hat{\mathbf{g}}^{(\theta)} - \mathbf{g}^{(\theta)}\right\|_2^2} \leq \sqrt{\frac{KL}{Q}} \|\mathbf{P}^{-1}\| \|\hat{\mathbf{x}} - \mathbf{x}\|_2 . \tag{73}$$

We now consider case 1 of the theorem, i.e., the use of G-BPDN for MGCS reconstruction. Recall (23), i.e., the fact that the G-RIC of the stacked measurement matrix $\mathbf{\Phi}$ in (20) with respect to the associated partition $\tilde{\mathcal{J}}$ defined in (19) satisfies $\delta_{S|\tilde{\mathcal{J}}} = \max_s \delta^{(s)}_{S|\mathcal{J}}$. Our assumption on the $\mathbf{\Phi}^{(s)}$, i.e., $\delta^{(s)}_{2S|\mathcal{J}} \leq \sqrt{2}-1$ for all $s \in \{1,\ldots,N_\mathrm{T}\}$, then implies that $\delta_{2S|\tilde{\mathcal{J}}} \leq \sqrt{2}-1$. Thus, with our additional assumption that $\sqrt{\sum_{\theta\in\Theta} \|\mathbf{z}^{(\theta)}\|_2^2} \leq \epsilon$, we have (cf. (15)) $\|\hat{\mathbf{x}} - \mathbf{x}\|_2 \leq \frac{c_0}{\sqrt{S}} \|\mathbf{x} - \mathbf{x}^{S|\tilde{\mathcal{J}}}\|_{2|\tilde{\mathcal{J}}} + c_1\epsilon$. Inserting into (73) yields the bound

$$E \leq \sqrt{\frac{KL}{Q}} \|\mathbf{P}^{-1}\| \left(\frac{c_0}{\sqrt{S}} \|\mathbf{x} - \mathbf{x}^{S|\tilde{\mathcal{J}}}\|_{2|\tilde{\mathcal{J}}} + c_1\epsilon\right). \tag{74}$$

Now recall the definition of $\mathbf{x}^{S|\tilde{\mathcal{J}}}$ in Section III-A as the vector minimizing $\|\mathbf{x} - \mathbf{x}'\|_{2|\tilde{\mathcal{J}}}$ among all group S-sparse vectors $\mathbf{x}' \in \Sigma_{S|\tilde{\mathcal{J}}}$, and note that the subvectors $\mathbf{x}^{S|\tilde{\mathcal{J}}}[b]$ coincide with the subvectors $\mathbf{x}[b]$ for $b \in \mathcal{T}$, where $\mathcal{T} \subseteq \{1,\ldots,B\}$ denotes the set of those S group indices that yield the largest norms $\|\mathbf{x}[b]\|_2$, and $\mathbf{x}^{S|\tilde{\mathcal{J}}}[b] = \mathbf{0}$ for $b \notin \mathcal{T}$. Therefore,

$$\left\|\mathbf{x} - \mathbf{x}^{S|\tilde{\mathcal{J}}}\right\|_{2|\tilde{\mathcal{J}}} = \sum_{b=1}^{B} \left\|\mathbf{x}[b] - \mathbf{x}^{S|\tilde{\mathcal{J}}}[b]\right\|_2 = \sum_{b\notin\mathcal{T}} \|\mathbf{x}[b]\|_2 . \tag{75}$$

Moreover, by the definition of $\mathcal{T}$, we have $\|\mathbf{x}[b]\|_2 \geq \|\mathbf{x}[b']\|_2$ for all $b \in \mathcal{T}$ and $b' \notin \mathcal{T}$, which yields $\sum_{b\in\mathcal{T}} \|\mathbf{x}[b]\|_2 \geq \sum_{b\in\mathcal{T}'} \|\mathbf{x}[b]\|_2$ for any set $\mathcal{T}' \subseteq \{1,\ldots,B\}$ of cardinality $|\mathcal{T}'| = |\mathcal{T}| = S$, and in turn $\sum_{b\notin\mathcal{T}} \|\mathbf{x}[b]\|_2 \leq \sum_{b\notin\mathcal{T}'} \|\mathbf{x}[b]\|_2$. Inserting into (75) gives

$$\left\|\mathbf{x} - \mathbf{x}^{S|\tilde{\mathcal{J}}}\right\|_{2|\tilde{\mathcal{J}}} \leq \sum_{b\notin\mathcal{T}'} \|\mathbf{x}[b]\|_2 , \tag{76}$$

for any such set $\mathcal{T}'$ of cardinality S. Then, with $\mathcal{S}$ defined as in Section IV-C, we obtain

$$\left\|\mathbf{x} - \mathbf{x}^{S|\tilde{\mathcal{J}}}\right\|_{2|\tilde{\mathcal{J}}} \overset{(a)}{\leq} \sum_{b\notin\mathcal{S}} \|\mathbf{x}[b]\|_2 \overset{(22)}{=} \sum_{b\notin\mathcal{S}} \sqrt{\sum_{\theta\in\Theta} \left\|\mathbf{x}^{(\theta)}[b]\right\|_2^2} \overset{(71)}{=} \sqrt{\frac{Q}{JD}} \sum_{b\notin\mathcal{S}} \sqrt{\sum_{\theta\in\Theta} \left\|\tilde{\mathbf{g}}^{(\theta)}[b]\right\|_2^2} , \tag{77}$$

where (a) follows from (76) and the fact that $|\mathcal{S}| = S$. Now for each group $\mathcal{I}_b$ of $\mathcal{J}$ we have (with $\mathcal{B}_b = \mathsf{S}^{-1}(\mathcal{I}_b)$, cf. (54) and the discussion following (54))

$$\sum_{\theta\in\Theta} \big\|\tilde{\mathbf{g}}^{(\theta)}[b]\big\|_2^2 \overset{(a)}{=} \sum_{\theta\in\Theta} \sum_{(m,i)\in\mathcal{B}_b} |\tilde{G}_{m,i}^{(\theta)}|^2 \overset{(b)}{=} \sum_{(m,i)\in\mathcal{B}_b} \big\|\tilde{\mathbf{G}}_{m,i}\big\|_{\mathrm{F}}^2 \overset{(c)}{\leq} \sum_{(m,i)\in\mathcal{B}_b} \|\mathbf{G}_{m,i}\|_{\mathrm{F}}^2 \|\mathbf{P}\|^2 \overset{(d)}{=} \|\mathbf{P}\|^2 \sum_{\theta\in\Theta} \big\|\mathbf{g}^{(\theta)}[b]\big\|_2^2 . \tag{78}$$

Here, (a) follows from $\tilde{\mathbf{g}}^{(\theta)} = \mathrm{rvec}_{m,i}\{\tilde{G}_{m,i}^{(\theta)}\}$, (b) follows from $\tilde{G}_{m,i}^{(r,s)} = \big[\tilde{\mathbf{G}}_{m,i}\big]_{r,s}$, (c) follows from $\tilde{\mathbf{G}}_{m,i} = \mathbf{G}_{m,i}\mathbf{P}$ and $\|\mathbf{AB}\|_{\mathrm{F}} \leq \|\mathbf{A}\|_{\mathrm{F}}\|\mathbf{B}\|$, and (d) follows from $\mathbf{g}^{(\theta)} = \mathrm{rvec}_{m,i}\{G_{m,i}^{(\theta)}\}$. Inserting (78) into (77) yields

$$\big\|\mathbf{x} - \mathbf{x}^{S|\tilde{\mathcal{J}}}\big\|_{2|\tilde{\mathcal{J}}} \leq \sqrt{\frac{Q}{JD}}\,\|\mathbf{P}\| \sum_{b\notin\mathcal{S}} \sqrt{\sum_{\theta\in\Theta} \big\|\mathbf{g}^{(\theta)}[b]\big\|_2^2} \overset{(a)}{=} \sqrt{\frac{Q}{JD}}\,\|\mathbf{P}\|\, C_{G,\mathcal{S},\mathcal{J}}\,, \tag{79}$$

where (a) follows from $\mathbf{g}^{(\theta)} = \mathrm{rvec}_{m,i}\{G_{m,i}^{(\theta)}\}$ and (32). Inserting this bound into (74) finally yields

$$E \leq c_0 \sqrt{\frac{KL}{JD}}\,\|\mathbf{P}^{-1}\|\,\|\mathbf{P}\|\,\frac{C_{G,\mathcal{S},\mathcal{J}}}{\sqrt{S}} + c_1 \sqrt{\frac{KL}{Q}}\,\|\mathbf{P}^{-1}\|\,\epsilon\,,$$

which is (34).

Next, we consider case 2, i.e., the use of G-CoSaMP for MGCS reconstruction. Under our assumption on the $\mathbf{\Phi}^{(s)}$, i.e., $\delta_{4S|\mathcal{J}}^{(s)} \leq 0.1$, the G-RIC of the stacked measurement matrix $\mathbf{\Phi}$ with respect to the associated partition $\tilde{\mathcal{J}}$ satisfies $\delta_{4S|\tilde{\mathcal{J}}} \leq 0.1$ (cf. (23) and the discussion above). With our additional assumption that $\sqrt{\sum_{\theta\in\Theta} \|\mathbf{z}^{(\theta)}\|_2^2} \leq \epsilon$, we obtain (cf. (16)) $\|\hat{\mathbf{x}} - \mathbf{x}\|_2 \leq \frac{1}{2^n}\|\mathbf{x}\|_2 + 20\big(1 + \frac{1}{\sqrt{S}}\big)\|\mathbf{x} - \mathbf{x}^{S|\tilde{\mathcal{J}}}\|_{2|\tilde{\mathcal{J}}} + 20\epsilon$. Inserting into (73) yields the bound

$$E \leq \sqrt{\frac{KL}{Q}}\,\|\mathbf{P}^{-1}\| \left[\frac{1}{2^n}\|\mathbf{x}\|_2 + 20\left(1 + \frac{1}{\sqrt{S}}\right)\big\|\mathbf{x} - \mathbf{x}^{S|\tilde{\mathcal{J}}}\big\|_{2|\tilde{\mathcal{J}}} + 20\epsilon\right]. \tag{80}$$

We have

$$\|\mathbf{x}\|_2^2 \overset{(22)}{=} \sum_{\theta\in\Theta} \big\|\mathbf{x}^{(\theta)}\big\|_2^2 \overset{(71)}{=} \frac{Q}{JD} \sum_{\theta\in\Theta} \big\|\tilde{\mathbf{g}}^{(\theta)}\big\|_2^2 . \tag{81}$$

Following a similar reasoning as in (78), we obtain

$$\sum_{\theta\in\Theta} \big\|\tilde{\mathbf{g}}^{(\theta)}\big\|_2^2 = \sum_{\theta\in\Theta} \sum_{m=0}^{D-1} \sum_{i=-J/2}^{J/2-1} \big|\tilde{G}_{m,i}^{(\theta)}\big|^2 = \sum_{m=0}^{D-1} \sum_{i=-J/2}^{J/2-1} \big\|\tilde{\mathbf{G}}_{m,i}\big\|_{\mathrm{F}}^2 \leq \sum_{m=0}^{D-1} \sum_{i=-J/2}^{J/2-1} \|\mathbf{G}_{m,i}\|_{\mathrm{F}}^2 \|\mathbf{P}\|^2 = \|\mathbf{P}\|^2 \sum_{\theta\in\Theta} \big\|\mathbf{g}^{(\theta)}\big\|_2^2 .$$

Thus, (81) becomes further

$$\|\mathbf{x}\|_2^2 \leq \frac{Q}{JD}\,\|\mathbf{P}\|^2 \sum_{\theta\in\Theta} \big\|\mathbf{g}^{(\theta)}\big\|_2^2 = \frac{Q}{JD}\|\mathbf{P}\|^2 \sum_{\theta\in\Theta} \sum_{m=0}^{D-1} \sum_{i=-J/2}^{J/2-1} \big|G_{m,i}^{(\theta)}\big|^2 . \tag{82}$$

Inserting (82) and (79) into (80), we finally obtain

$$E \le \frac{1}{2^n}\sqrt{\frac{KL}{JD}}\|\mathbf{P}^{-1}\|\|\mathbf{P}\|\sqrt{\sum_{\theta\in\Theta}\sum_{m=0}^{D-1}\sum_{i=-J/2}^{J/2-1}|G_{m,i}^{(\theta)}|^2} + 20\sqrt{\frac{KL}{JD}}\|\mathbf{P}^{-1}\|\|\mathbf{P}\|\,C_{G,\mathcal{S},\mathcal{J}}\left(1+\frac{1}{\sqrt{S}}\right) + \sqrt{\frac{KL}{Q}}\|\mathbf{P}^{-1}\|\,20\epsilon\,,$$

which is (35).

Appendix B: Proof of Inequality (52)

Supposing, without loss of generality, that $\|\mathbf{a}\|_2 \ge \|\mathbf{b}\|_2$, the inequality (52) is equivalent to

$$\left\|\frac{\mathbf{a}}{\|\mathbf{a}\|_2}-\frac{\mathbf{b}}{\|\mathbf{b}\|_2}\right\|_2^2 \le \frac{\|\mathbf{a}-\mathbf{b}\|_2^2}{\|\mathbf{b}\|_2^2}\,,$$

and, expanding the squared norms, to

$$2-2\frac{\mathbf{a}^T\mathbf{b}}{\|\mathbf{a}\|_2\|\mathbf{b}\|_2} \le \frac{\|\mathbf{a}\|_2^2+\|\mathbf{b}\|_2^2-2\mathbf{a}^T\mathbf{b}}{\|\mathbf{b}\|_2^2}\,.$$

Rearranging terms, this is furthermore equivalent to

$$\frac{\|\mathbf{a}\|_2^2}{\|\mathbf{b}\|_2^2}+2\frac{\mathbf{a}^T\mathbf{b}}{\|\mathbf{b}\|_2}\left(\frac{1}{\|\mathbf{a}\|_2}-\frac{1}{\|\mathbf{b}\|_2}\right)\ge 1\,. \tag{83}$$

To prove (83), we use the Cauchy-Schwarz inequality, noting that $\frac{1}{\|\mathbf{a}\|_2}-\frac{1}{\|\mathbf{b}\|_2}\le 0$:

$$\begin{aligned}\frac{\|\mathbf{a}\|_2^2}{\|\mathbf{b}\|_2^2}+2\frac{\mathbf{a}^T\mathbf{b}}{\|\mathbf{b}\|_2}\left(\frac{1}{\|\mathbf{a}\|_2}-\frac{1}{\|\mathbf{b}\|_2}\right) &\ge \frac{\|\mathbf{a}\|_2^2}{\|\mathbf{b}\|_2^2}+2\frac{\|\mathbf{a}\|_2\|\mathbf{b}\|_2}{\|\mathbf{b}\|_2}\left(\frac{1}{\|\mathbf{a}\|_2}-\frac{1}{\|\mathbf{b}\|_2}\right)\\ &= \frac{\|\mathbf{a}\|_2^2}{\|\mathbf{b}\|_2^2}+2\left(1-\frac{\|\mathbf{a}\|_2}{\|\mathbf{b}\|_2}\right)\\ &= \frac{\|\mathbf{a}\|_2^2}{\|\mathbf{b}\|_2^2}-2\frac{\|\mathbf{a}\|_2}{\|\mathbf{b}\|_2}+2\\ &= \left(\frac{\|\mathbf{a}\|_2}{\|\mathbf{b}\|_2}-1\right)^2+1\\ &\ge 1.\end{aligned}$$

Appendix C: Proof of Equation (60)

We will calculate the entries $G_{m,i}^{(\theta)}$ of $\mathbf{G}$ for elementary single-scatterer channels $h^{(\theta)}(t,\tau) = \delta(\tau-\tau_1^{(\theta)})\,e^{j2\pi\nu_1^{(\theta)}t}$, $\theta\in\Theta$. Combining (24) and (25) and using (55), we have

$$\sum_{m=0}^{D-1}\sum_{i=-J/2}^{J/2-1}\mathbf{G}_{m,i}\,\frac{1}{\sqrt{D}}\,v_{m,i}[\lambda]\,e^{-j2\pi\frac{\kappa m}{D}} = \sum_{m=0}^{D-1}\sum_{i=-J/2}^{J/2-1}\mathbf{F}_{m,i}\,e^{-j2\pi(\frac{\kappa m}{D}-\frac{\lambda i}{J})},$$

or, equivalently,

$$\frac{1}{\sqrt{D}} \sum_{i=-J/2}^{J/2-1} \mathbf{G}_{m,i}\, v_{m,i}[\lambda] \;=\; \sum_{i=-J/2}^{J/2-1} \mathbf{F}_{m,i}\, e^{j2\pi \frac{\lambda i}{J}}\,.$$

Expressing the $\mathbf{F}_{m,i}$ by (11), the previous relation written entrywise becomes

$$\frac{1}{\sqrt{D}} \sum_{i=-J/2}^{J/2-1} G^{(\theta)}_{m,i}\, v_{m,i}[\lambda] \;=\; \sum_{i=-J/2}^{J/2-1} \sum_{q=0}^{N-1} S^{(\theta)}_{h}[m, i+qL]\, A^{*}_{\gamma,g}\!\left(m, \frac{i+qL}{L_{\mathrm{r}}}\right) e^{j2\pi \frac{\lambda i}{J}}\,, \qquad \theta \in \Theta\,.$$

Inserting (42) (specialized to $P=1$, i.e., a single-scatterer channel with $\eta_1^{(\theta)} = 1$) and (43) yields

$$\frac{1}{\sqrt{D}} \sum_{i=-J/2}^{J/2-1} G^{(\theta)}_{m,i}\, v_{m,i}[\lambda] \;=\; \phi^{(\nu_1^{(\theta)})}\!\left(m - \frac{\tau_1^{(\theta)}}{T_{\mathrm{s}}}\right) C^{(\nu_1^{(\theta)})}[m, \lambda]\,,$$

with $C^{(\nu)}[m,\lambda]$ as defined in (59). Since $\{v_{m,i}[\lambda]\}_{i=-J/2}^{J/2-1}$ is an orthonormal basis, the last relation is equivalent to the following expression of $G^{(\theta)}_{m,i}$:

$$G^{(\theta)}_{m,i} \;=\; \sqrt{D}\, \phi^{(\nu_1^{(\theta)})}\!\left(m - \frac{\tau_1^{(\theta)}}{T_{\mathrm{s}}}\right) \sum_{\lambda=0}^{J-1} v^{*}_{m,i}[\lambda]\, C^{(\nu_1^{(\theta)})}[m, \lambda]\,.$$

For $\theta = \theta_\xi$ with $\xi \in \{1, \ldots, N_{\mathrm{T}} N_{\mathrm{R}}\}$, this can be rewritten as

$$G^{(\theta_\xi)}_{m,i} \;=\; \big[\mathbf{V}_m \mathbf{c}_m\big(\tau_1^{(\theta_\xi)}, \nu_1^{(\theta_\xi)}\big)\big]_{i+J/2+1} \;=\; \big[\mathbf{V}\mathbf{c}\big(\tau_1^{(\theta_\xi)}, \nu_1^{(\theta_\xi)}\big)\big]_{\mathsf{S}(m,i)} \;=\; \big[\mathbf{V}\mathbf{C}(\boldsymbol{\tau}_1, \boldsymbol{\nu}_1)\big]_{\mathsf{S}(m,i),\xi}\,,$$

and finally, because $G^{(\theta_\xi)}_{m,i} = [\mathbf{G}]_{\mathsf{S}(m,i),\xi}$ (see (56)), as

$$\mathbf{G} = \mathbf{V}\mathbf{C}(\boldsymbol{\tau}_1, \boldsymbol{\nu}_1).$$

REFERENCES

[1] E. Telatar, "Capacity of multi-antenna Gaussian channels," *European Trans. Telecomm.*, vol. 10, pp. 585–596, Nov. 1999.

[2] A. Paulraj, R. U. Nabar, and D. Gore, *Introduction to Space-Time Wireless Communications*. Cambridge (UK): Cambridge Univ. Press, 2003.

[3] E. Biglieri, R. Calderbank, A. Constantinides, A. Goldsmith, A. Paulraj, and H. V. Poor, *MIMO Wireless Communications*. Cambridge (UK): Cambridge University Press, 2010.

[4] E. J. Candès, J. Romberg, and T. Tao, "Robust uncertainty principles: Exact signal reconstruction from highly incomplete frequency information," *IEEE Trans. Inf. Theory*, vol. 52, pp. 489–509, Feb. 2006.

[5] D. L. Donoho, "Compressed sensing," *IEEE Trans. Inf. Theory*, vol. 52, pp. 1289–1306, Apr. 2006.

[6] S. Foucart and H. Rauhut, *A Mathematical Introduction to Compressive Sensing*. Applied and Numerical Harmonic Analysis, Basel, Switzerland: Birkhäuser, 2013.

[7] http://www.dsp.ece.rice.edu/cs/.

[8] G. L. Stuber, J. R. Barry, S. W. McLaughlin, Y. Li, M. A. Ingram, and T. G. Pratt, "Broadband MIMO-OFDM wireless communications," *Proc. IEEE*, vol. 92, pp. 271–294, Feb. 2004.

[9] M. Jiang and L. Hanzo, "Multiuser MIMO-OFDM for next-generation wireless systems," *Proc. IEEE*, vol. 95, pp. 1430–1469, Jul. 2007.

[10] IEEE P802 LAN/MAN Committee, "The working group for wireless local area networks (WLANs)." http://grouper.ieee.org/groups/802/11/index.html.

[11] IEEE P802 LAN/MAN Committee, "The working group on broadband wireless access standards." http://grouper.ieee.org/groups/802/16/index.html.

[12] http://www.3gpp.org/article/lte.

[13] J. Jayakumari, "MIMO-OFDM for 4G wireless systems," *Int. J. Eng. Sc. Tech.*, vol. 2, pp. 2886–2889, Jul. 2010.

[14] K. P. Bagadi and S. Das, "MIMO-OFDM channel estimation using pilot carries," *Int. J. Comp. Appl.*, vol. 2, pp. 81–88, May 2010.

[15] Y. Li, L. Cimini, and N. Sollenberger, "Robust channel estimation for OFDM systems with rapid dispersive fading channels," *IEEE Trans. Comm.*, vol. 46, pp. 902–915, Jul. 1998.

[16] Y. Li, N. Seshadri, and S. Ariyavisitakul, "Channel estimation for OFDM systems with transmitter diversity in mobile wireless channels," *IEEE J. Sel. Areas Comm.*, vol. 17, pp. 461–471, Mar. 1999.

[17] W. G. Jeon, K. H. Paik, and Y. S. Cho, "An efficient channel estimation technique for OFDM systems with transmitter diversity," in *Proc. IEEE PIMRC-00*, vol. 2, (London, UK), pp. 1246–1250, Sep. 2000.

[18] Y. Li, "Simplified channel estimation for OFDM systems with multiple transmit antennas," *IEEE Trans. Wireless Comm.*, vol. 1, pp. 67–75, Jan. 2002.

[19] I.-T. Lu and K.-J. Tsai, "Channel estimation in a proposed IEEE802.11n OFDM MIMO WLAN system," in *Proc. IEEE Sarnoff Symposium*, (Princeton, USA), pp. 1–5, April 2007.

[20] O. O. Oyerinde, *Channel Estimation for SISO and MIMO OFDM Communication Systems*. PhD thesis, University of KwaZulu-Natal, Durban, South Africa, Apr. 2010.

[21] G. Leus, Z. Tang, and P. Banelli, "Estimation of time-varying channels — A block approach," in *Wireless Communications over Rapidly Time-Varying Channels* (F. Hlawatsch and G. Matz, eds.), ch. 4, pp. 155–197, Academic Press, 2011.

[22] L. Rugini, P. Banelli, and G. Leus, "OFDM communications over time-varying channels," in *Wireless Communications over Rapidly Time-Varying Channels* (F. Hlawatsch and G. Matz, eds.), ch. 7, pp. 285–336, Academic Press, 2011.

[23] I. Barhumi, G. Leus, and M. Moonen, "Optimal training design for MIMO OFDM systems in mobile wireless channels," *IEEE Trans. Signal Processing*, vol. 51, pp. 1615–1624, Jun. 2003.

[24] H. Minn and N. Al-Dhahir, "Optimal training signals for MIMO OFDM channel estimation," *IEEE Trans. Wireless Comm.*, vol. 5, pp. 1158–1168, May 2006.

[25] M. Dong, B. M. Sadler, and L. Tong, "Pilot design and optimization for transmission over time-varying channels," in *Wireless Communications over Rapidly Time-Varying Channels* (F. Hlawatsch and G. Matz, eds.), ch. 5, pp. 199–236, Academic Press, 2011.

[26] G. Tauböck, F. Hlawatsch, D. Eiwen, and H. Rauhut, "Compressive estimation of doubly selective channels in multicarrier systems: Leakage effects and sparsity-enhancing processing," *IEEE J. Sel. Topics Signal Process.*, vol. 4, pp. 255–271, Apr. 2010.

[27] W. U. Bajwa, J. Haupt, A. M. Sayeed, and R. Nowak, "Compressed channel sensing: A new approach to estimating sparse multipath channels," *Proc. IEEE*, vol. 98, pp. 1058–1076, Jun. 2010.

[28] V. Raghavan, G. Hariharan, and A. M. Sayeed, "Capacity of sparse multipath channels in the ultra-wideband regime," *IEEE J. Sel. Areas Comm.*, vol. 1, pp. 357–371, Oct. 2007.

[29] S. F. Cotter and B. D. Rao, "Sparse channel estimation via matching pursuit with application to equalization," *IEEE Trans. Comm.*, vol. 50, pp. 374–377, Mar. 2002.

[30] W. Li and J. C. Preisig, "Estimation of rapidly time-varying sparse channels," *IEEE J. Oceanic Eng.*, vol. 32, pp. 927–939, Oct. 2007.

[31] M. Sharp and A. Scaglione, "Application of sparse signal recovery to pilot-assisted channel estimation," in *Proc. IEEE ICASSP-2008*, (Las Vegas, NV), pp. 3469–3472, Apr. 2008.

[32] W. U. Bajwa, A. M. Sayeed, and R. Nowak, "Compressed sensing of wireless channels in time, frequency, and space," in *Proc. 42nd Asilomar Conf. Sig., Syst., Comp.*, (Pacific Grove, CA), pp. 2048–2052, Oct. 2008.

[33] D. Eiwen, G. Tauböck, F. Hlawatsch, and H. G. Feichtinger, "Group sparsity methods for compressive channel estimation in doubly dispersive multicarrier systems," in *Proc. IEEE SPAWC-2010*, (Marrakech, Morocco), pp. 1–5, Jun. 2010.

[34] D. Eiwen, G. Tauböck, F. Hlawatsch, H. Rauhut, and N. Czink, "Multichannel-compressive estimation of doubly selective channels in MIMO-OFDM systems: Exploiting and enhancing joint sparsity," in *Proc. IEEE ICASSP-10*, (Dallas, TX), pp. 3082–3085, Mar. 2010.

[35] E. van den Berg, M. Schmidt, M. P. Friedlander, and K. Murphy, "Group sparsity via linear-time projection," Tech. Rep. TR-2008-09, University of British Columbia, Department of Computer Science, Jun. 2008.

[36] Y. C. Eldar and M. Mishali, "Robust recovery of signals from a structured union of subspaces," *IEEE Trans. Inf. Theory*, vol. 55, pp. 5302–5316, Nov. 2009.

[37] M. Stojnic, F. Parvaresh, and B. Hassibi, "On the reconstruction of block-sparse signals with an optimal number of measurements," *IEEE Trans. Signal Processing*, vol. 57, pp. 3075–3085, Aug. 2009.

[38] Y. C. Eldar, P. Kuppinger, and H. Bölcskei, "Compressed sensing of block-sparse signals: Uncertainty relations and efficient recovery," *IEEE Trans. Signal Processing*, vol. 58, pp. 3042–3054, Jun. 2010.

[39] R. G. Baraniuk, V. Cevher, M. F. Duarte, and C. Hegde, "Model-based compressive sensing," *IEEE Trans. Inf. Theory*, vol. 56, pp. 1982–2001, Apr. 2010.

[40] J. Chen and X. Huo, "Theoretical results on sparse representations of multiple-measurement vectors," *IEEE Trans. Signal Processing*, vol. 54, pp. 4634–4643, Dec. 2006.

[41] J. A. Tropp, A. C. Gilbert, and M. J. Strauss, "Algorithms for simultaneous sparse approximation. Part I: Greedy pursuit," *Signal Processing*, vol. 86, pp. 572–588, Mar. 2006.

[42] J. A. Tropp, "Algorithms for simultaneous sparse approximation. Part II: Convex relaxation," *Signal Processing*, vol. 86, pp. 589–602, Mar. 2006.

[43] R. Gribonval, H. Rauhut, K. Schnass, and P. Vandergheynst, "Atoms of all channels, unite! Average case analysis of multi-channel sparse recovery using greedy algorithms," *J. Fourier Anal. Appl.*, vol. 14, pp. 655–687, Dec. 2008.

[44] M. F. Duwarte, S. Sarvotham, D. Baron, M. B. Wakin, and R. G. Baraniuk, "Distributed compressed sensing of jointly sparse signals," in *Proc. 39th Asilomar Conf. Sig., Syst., Comp.*, (Pacific Grove, CA), pp. 3469–3472, Nov. 2005.

[45] W. Kozek and A. F. Molisch, "Nonorthogonal pulseshapes for multicarrier communications in doubly dispersive channels," *IEEE J. Sel. Areas Comm.*, vol. 16, pp. 1579–1589, Oct. 1998.

[46] G. Matz, D. Schafhuber, K. Gröchenig, M. Hartmann, and F. Hlawatsch, "Analysis, optimization, and implementation of low-interference wireless multicarrier systems," *IEEE Trans. Wireless Comm.*, vol. 6, pp. 1921–1931, May 2007.

[47] G. Matz, "Characterization and analysis of doubly dispersive MIMO channels," in *Proc. 40th Asilomar Conf. Sig., Syst., Comp.*, (Pacific Grove, CA), pp. 946–950, Oct. 2006.

[48] G. Matz and F. Hlawatsch, "Fundamentals of time-varying communication channels," in *Wireless Communications over Rapidly Time-Varying Channels* (F. Hlawatsch and G. Matz, eds.), ch. 1, pp. 1–53, Academic Press, 2011.

[49] P. A. Bello, "Characterization of randomly time-variant linear channels," *IEEE Trans. Comm. Syst.*, vol. 11, pp. 360–393, 1963.

[50] P. Flandrin, *Time-Frequency/Time-Scale Analysis*. San Diego (CA): Academic Press, 1999.

[51] J. A. Tropp, "Just relax: Convex programming methods for identifying sparse signals," *IEEE Trans. Inf. Theory*, vol. 51, pp. 1030–1051, Mar. 2006.

[52] E. J. Candès, J. Romberg, and T. Tao, "Stable signal recovery from incomplete and inaccurate measurements," *Comm. Pure Appl. Math.*, vol. 59, pp. 1207–1223, Mar. 2006.

[53] D. L. Donoho, M. Elad, and V. N. Temlyakov, "Stable recovery of sparse overcomplete representations in the presence of noise," *IEEE Trans. Inf. Theory*, vol. 52, pp. 6–18, Jan. 2006.

[54] Y. C. Pati, R. Rezaiifar, and P. S. Krishnaprasad, "Orthogonal Matching Pursuit: Recursive function approximation with applications to wavelet decomposition," in *Proc. 27th Asilomar Conf. Sig., Syst., Comp.*, vol. 1, (Pacific Grove, CA), pp. 40–44, Nov. 1997.

[55] G. Davis, S. Mallat, and M. Avellaneda, "Adaptive greedy approximation," *Constr. Approx.*, vol. 13, pp. 57–98, Jan. 1997.

[56] J. A. Tropp, "Greed is good: Algorithmic results for sparse approximation," *IEEE Trans. Inf. Theory*, vol. 50, pp. 2231–2242, Oct. 2004.

[57] J. A. Tropp and D. Needell, "CoSaMP: Iterative signal recovery from incomplete and inaccurate samples," *Appl. Comput. Harmon. Anal.*, vol. 26, pp. 301–321, May 2009.

[58] Z. Ben-Haim and Y. C. Eldar, "Near-oracle performance of greedy block-sparse estimation techniques from noisy measurements," *IEEE J. Sel. Topics Signal Process.*, vol. 5, pp. 1032–1047, Sep. 2011.

[59] A. C. Lozano, G. Świrszcz, and N. Abe, "Grouped orthogonal matching pursuit for variable selection and prediction," in *Proc. 23rd Ann. Conf. Neural Inf. Proc. Systems (NIPS)*, (Vancouver, Canada), pp. 1150–1158, Dec. 2009.

[60] E. J. Candès and T. Tao, "Decoding by linear programming," *IEEE Trans. Inf. Theory*, vol. 51, pp. 4203–4215, Dec. 2005.

[61] E. J. Candès, "The restricted isometry property and its implications for compressed sensing," *C. R. Acad. Sci. Paris, Ser. I*, vol. 346, pp. 589–592, May 2008.

[62] H. Rauhut and R. Ward, "Interpolation via weighted l1 minimization," *preprint*, 2013. arXiv:1308.0759 [math.FA].

[63] E. J. Candès and T. Tao, "Near-optimal signal recovery from random projections: Universal encoding strategies?," *IEEE Trans. Inf. Theory*, vol. 52, pp. 5406–5425, Dec. 2006.

[64] M. Rudelson and R. Vershynin, "On sparse reconstruction from Fourier and Gaussian measurements," *Communications on Pure and Applied Mathematics*, vol. 61, no. 8, pp. 1025–1045, 2008.

[65] M. F. Duarte, V. Cevher, and R. G. Baraniuk, "Model-based compressive sensing for signal ensembles," in *Proc. 47th Ann. Allerton Conf. Communication, Control, Computing*, (Monticello, IL), pp. 244–250, Sep. 2009.

[66] S. F. Cotter, B. D. Rao, K. Engan, and K. Kreutz-Delgado, "Sparse solutions to linear inverse problems with multiple measurement vectors," *IEEE Trans. Signal Processing*, vol. 53, pp. 2477–2488, Jul. 2005.

[67] R. A. Horn and C. R. Johnson, *Matrix Analysis*. Cambridge (UK): Cambridge Univ. Press, 1999.

[68] T. Blumensath and M. E. Davies, "Gradient pursuits," *IEEE Trans. Signal Processing*, vol. 56, pp. 2370–2382, Jun. 2008.

[69] A. F. Molisch, ed., *Wideband Wireless Digital Communications*. Englewood Cliffs (NJ): Prentice Hall, 2001.

[70] J. Karedal, F. Tufvesson, N. Czink, A. Paier, C. Dumard, T. Zemen, C. Mecklenbrauker, and A. Molisch, "A geometry-based stochastic MIMO model for vehicle-to-vehicle communications," *IEEE Trans. Wireless Comm.*, vol. 8, no. 7, pp. 3646–3657, 2009.

[71] N. Czink, T. Zemen, J.-P. Nuutinen, J. Ylitalo, and E. Bonek, "A time-variant MIMO channel model directly parametrised from measurements," *EURASIP J. Wirel. Commun. Netw.*, vol. 2009, pp. 4:1–4:16, Feb. 2009.
[72] A. F. Molisch, *Wireless Communications*. Chichester (UK): Wiley, 2005.
[73] G. H. Golub and C. F. Van Loan, *Matrix Computations*. Baltimore (MD): Johns Hopkins University Press, 2nd ed., 1989.
[74] S. Boyd and L. Vandenberghe, *Convex Optimization*. Cambridge (UK): Cambridge Univ. Press, 2004.
[75] G. Del Galdo and M. Haardt, "IlmProp: A flexible geometry-based simulation environment for multiuser MIMO communications," in *COST 273 Temporary Document, No. TD(03)188*, (Prague, Czech Republic), Sep. 2003.
[76] Y. C. Eldar and H. Rauhut, "Average case analysis of multichannel sparse recovery using convex relaxation," *IEEE Trans. Inf. Theory*, vol. 56, pp. 505–519, Jan. 2010.
[77] X. He, R. Song, and W.-P. Zhu, "Pilot allocation for sparse channel estimation in MIMO-OFDM systems," *IEEE Trans. Circuits Systems II: Express Briefs*, vol. 60, no. 9, pp. 612–616, 2013.
[78] M. Gay, A. Lampe, and M. Breiling, "Sparse OFDM channel estimation based on regular pilot grids," in *Proc. 9th Int. ITG Conf. Systems, Commun., Coding (SCC)*, pp. 1–6, 2013.
[79] D. Eiwen, G. Tauböck, F. Hlawatsch, and H. G. Feichtinger, "Compressive tracking of doubly selective channels in multicarrier systems based on sequential delay-Doppler sparsity," in *Proc. IEEE ICASSP-11*, (Prague, Czech Republic), pp. 2928–2931, May 2011.